Caspase-11 drives macrophage hyperinflammation in models of Polg-related mitochondrial disease

Jordyn J. VanPortfliet[1,2], Yuanjiu Lei[2,3], Camila Guerra Martinez[2], Jessica Wong[1], Kathryn Pflug[4], Raquel Sitcheran[4], Stephen C. Kneeland[1], Stephen A. Murray[1], Peter. J. McGuire[5], Carolyn L. Cannon[2], A. Phillip West[1,2,*]

[1]The Jackson Laboratory, Bar Harbor, Maine 04609, USA

[2]Department of Microbial Pathogenesis and Immunology, School of Medicine, Texas A&M University, Bryan, Texas 77807, USA

[3]Department of Pathology, Yale School of Medicine, New Haven, CT 06520, USA

[4]Department of Cell Biology and Genetics, School of Medicine, Texas A&M University, Bryan, Texas 77807, USA

[5]Metabolism, Infection and Immunity Section, National Human Genome Research Institute, National Institutes of Health, Bethesda, Maryland, 20892, USA

* Correspondence to: phillip.west@jax.org

Abstract

Mitochondrial diseases (MtD) represent a significant public health challenge due to their heterogenous clinical presentation, often severe and progressive symptoms, and the lack of effective therapies. Environmental exposures, such bacterial and viral infection, can further compromise mitochondrial function and exacerbate the progression of MtD. Infections in MtD patients more frequently progress to sepsis, pneumonia, and other detrimental inflammatory endpoints. However, the underlying immune alterations that enhance immunopathology in MtD remain unclear, constituting a key gap in knowledge that complicates treatment and increases mortality in this population. Here we employ in vitro and in vivo approaches to clarify the molecular and cellular basis for innate immune hyperactivity in models of polymerase gamma (Polg)-related MtD. We reveal that type I interferon (IFN-I)-mediated upregulation of caspase-11 and guanylate-binding proteins (GBPs) increase macrophage sensing of the opportunistic microbe *Pseudomonas aeruginosa* (PA) in Polg mutant mice. Furthermore, we show that excessive macrophage cytokine secretion and pyroptotic cell death contribute to lung inflammation and morbidity after infection with PA. Our work sheds new light on innate immune dysregulation in MtD and reveals potential targets for limiting infection- and inflammation-related complications in Polg-related MtD.

Introduction

Mitochondrial diseases (MtD) are the most common inborn error of metabolism and are caused by deleterious variants in genes that function in oxidative phosphorylation (OXPHOS) and mitochondrial DNA (mtDNA) maintenance[1]. MtD can present at any age, vary in severity, and display clinical heterogeneity with differing degrees of organ system involvement[2,3]. Although the genetic basis of MtD is becoming more clear, the underlying mechanisms that cause pathology, as well as the contribution of environmental factors to disease progression, are less clear. Notably, viral and bacterial infections may unmask MtD or hasten the stepwise progression of disease by triggering metabolic decompensation, a dangerous deterioration in mitochondrial function[4]. Clinical evidence suggests that patients with MtD are highly susceptible to infection by opportunistic respiratory pathogens. Moreover, pneumonia and microbial sepsis are the primary causes of early death in pediatric patients, and some adults, with MtD[5,6]. Thus, there is ample evidence highlighting the damaging toll of infection in MtD[7]. However, the underlying immune alterations that drive immunopathology and prevent proper control of infection represent a significant knowledge gap that complicates treatment and enhances morbidity and mortality in this vulnerable patient population.

In addition to their bioenergetic functions, mitochondria are key metabolic and signaling hubs in the mammalian immune system[8]. Mitochondria are also important sources of damage-associated molecular patterns (DAMPs), such as mtDNA, which engage innate immune signaling when released from the organelle and are linked to inflammation in a growing number of human diseases[9,10]. There is growing appreciation for a bidirectional relationship between MtD and inflammation, where mitochondrial dysfunction in MtD activates the innate immune system leading to inflammatory responses that further compromise mitochondrial activity[11]. In

agreement with this hypothesis, elevated inflammatory cytokines have been observed in patients with Polymerase gamma (Polg)-related Alpers-Huttenlocher syndrome[12], Barth syndrome[13], and Friedreich ataxia[14,15]. Animal models have also revealed innate immune system dysregulation as a frequent feature of MtD. For example, the *Ndufs4*$^{-/-}$ mouse model of neurodegeneration and Leigh syndrome exhibits increased circulating pro-inflammatory cytokines along with macrophage and microglial activation[16–19].

We recently uncovered that the Polg^{D257A} mutator model of mtDNA instability exhibits a hyperinflammatory innate immune status due to chronic engagement of the cyclic GMP-AMP synthase (cGAS)—Stimulator of Interferon Genes (STING)—type one interferon (IFN-I) axis[20]. Notably, we reported that persistent IFN-I signaling in these mice causes widespread repression of the antioxidant and anti-inflammatory transcription factor nuclear factor erythroid 2-related factor 2 (Nrf2)[21,22] in myeloid immune cells and organs of the Polg^{D257A} mouse. Consequently, Polg^{D257A} mice are more sensitive to septic shock caused by intraperitoneal injection of a high dose of lipopolysaccharide (LPS)[20]. Although Polg^{D257A} mutator mice do not phenocopy any particular human MtD, these animals present pathology overlapping the MtD spectrum, including hearing loss, cardiomyopathy, progressive anemia, and lymphopenia[23–25]. Moreover, increased susceptibility to septic shock and elevated inflammatory and IFN-I signatures are common features of both Polg mutator mice and patients with diverse MtD[11].

Overall, our prior work provided foundational evidence linking mitochondrial dysfunction to hyperinflammatory innate immune signaling in the Polg^{D257A} model of MtD. However, there remains a critical need to expand these findings into relevant infection models, given the high rate of infections that frequently lead to innate immune hyperactivity and sepsis in MtD. *Pseudomonas aeruginosa* (PA) is a common opportunistic pathogen of concern in MtD as

infection can lead to sepsis and pneumonia[6]. PA is a robust activator of innate immunity in the respiratory tract, and lung colonization by PA drives persistent recruitment of monocytes and neutrophils leading to pneumonia, lung injury, and/or systemic bacterial spread[26,27]. PA is especially problematic in MtD due to the prevalence of antibiotic resistant strains, abundance in hospitals, and high rate of recurrence[26,28,29]. Thus, it is important to define how PA and other opportunistic bacteria engages the innate immune system in MtD to define immunomodulatory strategies that boost anti-bacterial immunity, while limiting hyperinflammation that may hasten metabolic decompensation and disease progression.

In this study, we utilized in vitro and in vivo PA infection models to characterize the underlying innate immune mechanisms governing hyperinflammation in Polg^{D257A} mice. We also report a new mouse model that incorporates a pathogenic Polg variant observed in humans. We reveal that both Polg mutant models exhibit excessive macrophage inflammasome activation, cytokine secretion, and pyroptotic cell death, which contribute to inflammation, acute lung injury, and morbidity after infection with PA. These findings further advance knowledge of how mitochondrial dysfunction impacts innate immune responses during bacterial infection and Polg-related diseases and reveals innate immune targets for limiting infection- and inflammation-related complications in MtD.

Results

Polg mutant macrophages exhibit increased IFN-I and pro-inflammatory responses after bacterial challenge

Our recent work uncovered that elevated IFN-I and repression of Nrf2 signaling augment innate immune activity and inflammation in Polg^{D257A} mice challenged with Toll-like receptor

(TLR) agonist, LPS[20]. We hypothesized that the hyperinflammatory phenotype of Polg^{D257A} mice might be further exacerbated during bacterial infection. Therefore, we challenged bone marrow-derived macrophages (BMDMs) with *Pseudomonas aeruginosa* strain O1 (PAO1) (Fig. 1a) and performed RNA sequencing (RNAseq) and pathway analysis (Fig. 1b). Similar to BMDMs treated with LPS[20], PAO1-challenged Polg^{D257A} BMDMs displayed heightened expression of pro-inflammatory cytokines, IFN-I, interferon-stimulated genes (ISGs), and innate immune signaling factors (Fig. 1c; Supplementary Fig. 1a). Gene Set Enrichment Analysis confirmed PAO1-infected Polg^{D257A} BMDMs exhibit more robust pro-inflammatory cytokine, chemokine, and IFN-I gene expression relative to wild-type (WT) BMDMs (Supplementary Fig. 1b). Additional experiments substantiated RNAseq datasets, revealing heightened expression of ISGs and pro-inflammatory cytokine secretion in PAO1-infected Polg^{D257A} peritoneal macrophages (PerMacs) and BMDMs over a one-day time course (Fig. 1d-e). Prior work from our lab showed that elevated IFN-I responses in Polg^{D257A} mice suppress Nrf2-mediated antioxidant and anti-inflammatory signaling[20]. We noted consistent activation of IFN-I signaling factors and a coordinated downregulation of Nrf2 target genes in PAO1-infected Polg^{D257A} macrophages (Fig. 1f-g). Addition of dimethyl fumarate (DMF), an anti-inflammatory and Nrf2 stabilizing agent[30,31], dramatically reduced IFN-I and inflammatory gene signatures in Polg^{D257A} macrophages during PAO1 challenge, while also restoring expression of Nrf2 target genes (Fig. 1b-c, f-h and Supplementary Fig. 1). Notably, DMF treatment reduced the hyperproduction of multiple pro-inflammatory cytokines in Polg^{D257A} PerMacs at both 8 and 24 hours post challenge (hpc) (Fig. 1i). In sum, our data highlight that Polg^{D257A} macrophages are hyperactivated by LPS and PAO1 and reveal that DMF inhibits inflammation and restores Nrf2 levels in Polg mutant cells.

Polg mutant macrophages exhibit potentiated cell death upon bacterial challenge

As we observed increased IL-1β secretion from Polg^{D257A} PerMacs, we next investigated inflammatory cell death pathways during PAO1 infection. RNAseq and pathway analysis revealed significant enrichment of genes involved in inflammasome signaling, immunogenic cell death, and death receptor signaling in Polg^{D257A} BMDMs after PAO1 challenge (Fig. 2a-b). Consistent with cell death gene expression patterns in BMDMs, Polg^{D257A} PerMacs stained weakly with the nuclear and plasma membrane dye CellMask HCS Deep Red and exhibited rapid condensation of nuclei after PAO1 challenge (Fig. 2c-d). Reduced CellMask staining was also observed in ASC positive WT BMDMs after LPS priming and nigericin treatment (Supplementary Fig. 2a-b), indicating that low CellMask staining marks cells undergoing pyroptosis. In line with increased pyroptotic cell death, Polg^{D257A} BMDMs more rapidly became propidium iodide (PI) positive (Fig. 2e) and secreted more IL-1β after incubation with PAO1 (Fig. 2f). We also noted elevated release of PAO1 into the culture supernatant of Polg^{D257A} BMDMs, concomitant with lower numbers of intracellular bacteria (Supplementary Fig. 2c). Reduced intracellular bacteria was not the result of impaired phagocytosis, as Polg^{D257A} BMDMs displayed no impairment in uptake of LPS coated fluorescent microspheres (Supplementary Fig. 2d-e).

DMF is a robust inhibitor of the NLRP3 inflammasome[32], and addition of DMF during PAO1 infection was sufficient to reduce genes governing cell death and heightened pyroptotic phenotypes in Polg^{D257A} macrophages (Fig. 2). In addition to activating NLRP3, PA can also activate the NLRC4 canonical inflammasome and the non-canonical caspase-11 inflammasome[27,33–35]. Culture of Polg^{D257A} BMDMs with non-pathogenic *E. coli* (DH5α), which

lack flagellin and therefore can only activate NLRP3 or caspase-11, also promoted increased IL-1β, TNFα, and IL-6 secretion (Supplementary Fig. 2f) and pyroptotic cell death (Supplementary Fig. 2g-h). Collectively, these data indicate that elevated cell death and cytokine secretion in Polg^{D257A} macrophages during bacterial challenge are not due to PAO1 virulence factors, but are likely caused by potentiated activation of NLRP3 and/or caspase-11 inflammasomes.

Elevated IFN-I potentiates expression and activation of the non-canonical caspase-11 inflammasome in Polg mutant macrophages

To further confirm a role for pyroptosis in hyperinflammation and increased cell death in Polg mutant macrophages, we incubated BMDMs with Ac-YVAD-cmk (AcYVAD), a selective caspase-1 inhibitor. AcYVAD nearly abrogated IL-1β secretion from Polg^{D257A} macrophages while also decreasing TNFα and IL-6 during PAO1 challenge (Fig. 3a). In contrast, QVD-OPH, a more potent inhibitor of apoptotic caspases, had minor effects on PAO1-induced cytokine secretion in Polg^{D257A} BMDMs (Fig. 3a). AcYVAD also reduced PI uptake in Polg^{D257A} BMDMs (Fig. 3b) and blunted pyroptotic phenotypes of Polg^{D257A} PerMacs (Fig. 3c-d) after incubation with PAO1. Polg^{D257A} BMDMs treated with LPS alone did not exhibit increased PI uptake, suggesting that priming is not sufficient to potentiate cell death (Supplementary Fig. 3a).

Given elevated pyroptosis in PAO1-infected Polg^{D257A} BMDMs, we next performed isolated challenge experiments to determine which inflammasome pathways were hyperactivated in mutant macrophages. Surprisingly, LPS priming followed by flagellin transfection to activate the NLRC4 inflammasome revealed that Polg^{D257A} macrophages exhibit reduced PI uptake and IL-1β secretion (Supplementary Fig. 3b-c). LPS priming followed by the addition of ATP also revealed modestly impaired NLRP3 inflammasome activation in Polg^{D257A} BMDMs, as

measured by PI uptake, IL-1β secretion, and caspase-1 cleavage (Supplementary Fig. 3d-f). LPS priming followed by nigericin treatment revealed similar impairments in NLRP3 inflammasome activity (Supplementary Fig. 3g-i). OXPHOS has recently been shown to be vital for NLRP3 activation in response to nigericin and other stimuli[36]. Polg^{D257A} BMDMs displayed reduced basal and maximal respiration at rest and after LPS challenge (Supplementary Fig. 3j-l), suggesting that reduced canonical inflammasome activation is likely due to OXPHOS impairment in Polg^{D257A} BMDMs.

Although Polg^{D257A} BMDMs exhibited reduced NLRP3 and NLRC4 responses when triggered with pure inflammasome activators, mutant BMDMs displayed elevated caspase-1 and Gasdermin D (GSDMD) cleavage, as well as increased caspase-11 and IL-1β expression, after incubation with PAO1 as compared with WT controls (Fig. 3e). Moreover, AcYVAD treatment inhibited the hypersecretion of IL-1β and other pro-inflammatory cytokines in Polg^{D257A} BMDMs challenged with PAO1 for 24 hours (Fig. 3f). Notably, IL-1α secretion was markedly higher in Polg^{D257A} macrophages after PAO1 challenge (Fig. 1i and 3f). IL-1α is an alarmin that feeds forward to augment production of other cytokines, and the robust secretion of IL-1α from myeloid cells involves caspase-11[37–39]. Thus, given elevated caspase-11 expression in Polg^{D257A} BMDMs, we next explored its involvement in cell death and cytokine secretion. After LPS priming followed by LPS transfection, Polg^{D257A} BMDMs rapidly became PI positive and secreted increased levels of IL-1β (Fig. 3g-h). Both phenotypes could be markedly inhibited by treatment with AcYVAD, indicating that heightened activation of caspase-11 triggers NLRP3 inflammasome and caspase-1 activation more robustly in Polg^{D257A} BMDMs (Fig. 3g-h). As caspase-11 activation requires IFN-I priming[40] and Polg^{D257A} macrophages and mice exhibit elevated IFN-I signaling[20], we reasoned that IFN-I is responsible for caspase-11 expression and

activation in Polg^{D257A} BMDMs. In agreement, we observed potentiated caspase-11 mRNA and protein after PAO1 infection (Fig. 3e, i). Notably, IFN alpha receptor (IFNAR) blockade using the MAR1-5A3 monoclonal antibody markedly reduced PI uptake after caspase-11 activation (Fig. 3j), while also lowering pro-inflammatory cytokine hyperproduction in PAO1-challenged Polg^{D257A} BMDMs (Supplementary Fig. 3m). Collectively, these data indicate that the IFN-I-dependent potentiation of caspase-11 mediates caspase-1-dependent pyroptosis and hyperinflammation in Polg^{D257A} macrophages exposed to PAO1.

Increased GBP expression and targeting to intracellular PAO1 in Polg^{D257A} macrophages

Prior work has shown that IFN-I signaling during bacterial infection drives the expression of guanylate binding proteins (GBPs)[41], which facilitate innate immune responses and non-canonical inflammasome activation by disrupting membranes of pathogen-containing vacuoles, or pathogens themselves, to liberate LPS or other PAMPs[34,42–44]. Consistent with elevated IFN-I signaling, RNA-seq analysis revealed more robust GBP expression in Polg^{D257A} BMDMs after challenge with PAO1 (Fig. 4a). Immunofluorescence microscopy revealed increased GBP5 expression in resting Polg^{D257A} BMDMs (Fig. 4b-c), as well as during PAO1 challenge (Fig. 4d-e). Notably, we observed a more robust colocalization of GBP5 with PAO1 challenged Polg^{D257A} macrophages after staining with an antibody specific for PA LPS (Fig. 4d, f). Intracellular PAO1 in Polg^{D257A} BMDMs colocalized strongly with GBP5 and appeared more aggregated with bacteria than in WT BMDMs. These findings suggest that elevated IFN-I in Polg^{D257A} macrophages augments GBP expression, likely enhancing sensing of LPS via caspase-11 that contributes to potentiated cell death and pro-inflammatory cytokine release.

A novel Polg^{R292C} mouse model incorporating a deleterious patient mutation exhibits macrophage mtDNA depletion, elevated IFN-I responses, increased pyroptosis, and hyper-inflammation after challenge with PAO1

To determine if our findings in Polg^{D257A} macrophages are more broadly applicable to other models of OXPHOS deficiency due to mtDNA perturbations, we leveraged a novel model of Polg-related mitochondrial disease harboring a single amino acid missense mutation (Arg292Cys) in exon 4 of the exonuclease domain of Polg (Fig. 5a), which is homologous to the human Arg309Cys (c.925C>T) pathogenic variant[45,46]. We generated these mice using CRISPR/Cas9 editing of ES cells and verified germline transmission of the mutation by sequencing (Fig. 5b). The Arg309Cys variant alone or in combination with other Polg variants causes reduced mtDNA copy number, mtDNA deletions, and severe phenotypes including mitochondrial myopathy, encephalopathy, lactic acidosis and stroke-like episodes (MELAS), peripheral neuropathy, ataxia, and epilepsy in patients. Although being born below expected mendelian ratios, homozygous Polg^{R292C} mice are viable (data not shown, data to be reported in subsequent manuscript). BMDMs derived from Polg^{R292C} mice did exhibit mtDNA depletion at rest (Fig. 5c), as well as lower numbers of nucleoids and fragmented mitochondrial networks after stimulation with LPS (Fig. 5d-e). In line with our data from the Polg^{D257A} mutator mice, Polg^{R292C} BMDMs displayed a constitutive elevation of ISGs at rest and potentiated ISG expression after LPS stimulation (Supplementary Fig. 4a-b). Moreover, Polg^{R292C} BMDMs exhibited increased ISG and GBP expression after challenge with PAO1 (Fig. 5f), while also exhibiting more pyroptosis (Fig. 5g-h) and pro-inflammatory cytokine secretion (Fig. 5i). These data suggest that elevated IFN-I, hyperinflammation, and cell death in response to PAO1 are

common features of macrophages harboring Polg exonuclease domain mutations, including the mitochondrial disease-relevant Arg292Cys variant.

Intratracheal instillation of a non-lethal dose of PAO1 elicits greater lung cytokine production and modest changes in lung immune cell populations in Polg mutant mice

Patients with primary MtD often experience recurrent viral and bacterial infections of the respiratory tract, including infections by PA[5]. These events can trigger metabolic decompensation and can progress to systemic inflammatory endpoints and/or sepsis. However, few studies have examined infection kinetics and lung immune responses in Polg-related mitochondrial disorders. We therefore employed intratracheal instillation protocols to administer LPS or PAO1 into the lungs of $Polg^{D257A}$ mutator mice. Histological analysis of resting $Polg^{D257A}$ lungs did not reveal obvious differences in morphology or cellular composition (Supplementary Fig. 4c-e), although consistent with our earlier findings[20], basal expression of ISGs were elevated compared to WT littermates (Supplementary Fig. 4f). After LPS was instilled into lungs through cannulation of the trachea, $Polg^{D257A}$ mice secreted more TNFα and IL-6 at all timepoints and increased IL-1β at the 12 hour timepoint in the bronchial alveolar lavage fluid (BAL) compared to WT mice (Supplementary Fig. 4g).

To next characterize lung innate immune responses to PAO1 infection in the $Polg^{D257A}$ mice, we challenged mice with a non-lethal dose of PAO1[47]. Both WT and $Polg^{D257A}$ mice infected with $1x10^4$ colony forming units (CFU) of PAO1 via intratracheal instillation lost weight initially, but returned to normal weight (Supplementary Fig. 5a) and exhibited no culturable bacteria (data not shown) 3 days post infection. Flow cytometric analysis of lung cells in BAL fluid revealed an overall decrease in the percentage of $CD45^+$ immune cells at rest and

after infection, consistent with general leukopenia noted in Polg^{D257A} mice[20,25] (Supplementary Fig. 5b-c). Analysis of specific immune cell markers on lung CD45^{+} cells revealed few changes in BAL populations (Supplementary Fig. 5d-l) between uninfected WT and Polg^{D257A} mice, although there were more SiglecF^{+} and F4/80^{+} cells at rest perhaps indicating elevated numbers of lung macrophages (Supplementary Fig. 5e,g). Six hours post infection, there was a marked reduction in SiglecF^{+} cells in Polg^{D257A} mice relative to WTs and an increase in CD3^{+} T cells (Supplementary Fig. 5e,i). Cells labeling with the neutrophil marker, Ly6G, were dramatically increased at 6 hours, although there were no differences between WT and Polg^{D257A} mice (Supplementary Fig. 5k). At 48 hours post infection, neutrophils remained the most predominant CD45^{+} population in both genotypes, but we observed a reversion toward increased numbers of cells staining positive for macrophage markers SiglecF^{+} and F4/80^{+} in Polg^{D257A} mice (Supplementary Fig. 5e,g,k).

Despite modest changes in cellular composition of the BAL fluid, Polg^{D257A} mice had elevated numbers of CD45^{+} cells expressing TNFα both at rest and six hours post infection (Supplementary Fig. 5m), consistent with increased TNFα production after LPS challenge. Multianalyte analysis of the BAL fluid using Legendplex assays revealed 2-4 fold increases in lung pro-inflammatory cytokines in Polg^{D257A} mice 6 hours post PAO1 infection (Fig. 6a). Consistent with resolution of infection in both genotypes, cytokine differences in the BAL of WT and Polg^{D257A} mice were less pronounced at 48 hours post infection (Supplementary Fig. 6a). However, IFNβ and inflammatory cytokines associated with the skewing and differentiation of T cell Th1 (IL-27) and Th17 subsets (IL-23) remained elevated in Polg^{D257A} mice in an IFNAR-dependent fashion (Supplementary Fig. 6a). Analysis of lung protein extracts revealed elevated caspase-1 cleavage, as well as increased caspase-11, NLRC4, and NLRP3 expression in

Polg^{D257A} mice 48 hours post intratracheal instillation of 1x10^{4} CFU of PAO1. GSDMD, GBP5, and other ISGs were also elevated in Polg^{D257A} lungs, consistent with sustained IFNβ expression observed by Legendplex (Fig. 6b).

Given that recurrent respiratory tract infections are often observed in patients with MtD, we next infected mice with 1x10^{4} CFU PAO1, followed by a 7-day rest period, then re-infected with 1x10^{4} CFU PAO1. Histological analysis of lungs 24 hours following re-infection revealed monocyte and granulocyte infiltration into lungs, areas of vascular hemorrhage, and more Eosin positive cells in Polg^{D257A} lungs relative to WT (Supplementary Fig. 6b-c). Lung IL-12 family cytokines and IFNβ were significantly higher in Polg^{D257A} mice at the 24 hour harvest point following re-infection, while other cytokines were trending higher in Polg^{D257A} mice, although they did not reach statistical significance (Supplementary Fig. 6d). We also observed higher bacterial burdens in the lungs and spleens of Polg^{D257A} mice compared to WT controls (Supplementary Fig. 6e). Altogether, these data indicate that Polg^{D257A} mice exhibit hyperinflammation and impaired antibacterial immunity upon re-infection with PAO1.

Intratracheal infection with a higher dose of PAO1 elicits greater lung immune cell infiltration, caspase-11 expression, and death of Polg mutant mice

We next utilized a higher dose of PAO1 to expand on low-dose data and assess mortality in Polg^{D257A} mice. Upon intratracheal instillation of 1x10^{5} CFU PAO1, Polg^{D257A} mutant mice displayed elevated neutrophilic inflammation and overall lung inflammatory scores via histological analysis (Fig. 6c-e) at 20 hours post infection, despite no differences in bacterial burden (Supplementary Fig. 6f). We also observed heightened expression of caspase-11 in lung lysates of Polg^{D257A} mutant mice (Fig. 6f), consistent with our findings in macrophages and lungs

exposed to lower doses of PAO1 (Fig. 6a-b). Moreover, pro-IL-1β and the mature cytokine were elevated in Polg^{D257A} lungs 20 hours after infection with 1x10^{5} CFU of PAO1 (Fig. 6f). Finally, we observed that a greater number of Polg^{D257A} mice reached a moribund state after infection with this higher dose of PAO1 relative to WT littermates (Fig. 6g). Overall, these in vivo data suggest that Polg^{D257A} mice are more prone to excessive inflammation and acute lung injury following infection with PAO1. We therefore conclude that macrophage and myeloid cell hyperinflammation driven by caspase-11 and other innate immune pathways promotes lung damage that alters antibacterial responses and increases mortality in the Polg^{D257A} model of mitochondrial dysfunction (Fig. 6h).

Discussion

Patients with MtD experience a greater frequency of bacterial and viral infections that can rapidly progress to sepsis or systemic inflammatory response syndrome (SIRS), leading to premature death[5]. Recurrent infections can also accelerate MtD progression by promoting metabolic decompensation, a life-threatening condition that hastens deterioration of mitochondrial function[48–50]. Polg is the sole mitochondrial DNA polymerase, and mutations in *POLG* are the most prevalent single-gene cause of MtD[51]. There are several clinical reports of bacterial or viral infections unmasking Polg-related MtD symptoms and hastening disease progression[52,53]. Moreover, one study revealed the presence of inflammatory cytokines in the cerebrospinal fluid of a patient with Polg-related MtD[12,19]. As cytokine-mediated toxicity is an important driver of metabolic decompensation[7], there is a critical need to understand immune responses in patients with Polg-related disorders and other MtD to manage infections and inflammation-related complications.

The present study builds upon our prior work to characterize innate immunity in mouse models of MtD[20,54] and leverages bacterial infection, cytokine profiling, histological analyses, and in vitro and ex vivo cellular assays to define macrophage inflammatory dynamics in Polg^{D257A} mutator mice. We also utilize macrophages from Polg^{R292C} mice that carry a mutation observed in patients to broaden our findings into a more faithful model of Polg-related MtD. Macrophages from Polg^{D257A} mutator and our novel Polg^{R292C} mice exhibit elevated ISG expression and secrete more pro-inflammatory cytokines after challenge with PA. Notably, inclusion of DMF, an immunomodulatory and Nrf2-stabilizing agent, during PAO1 challenge significantly reduced IFN-I and pro-inflammatory signatures. These findings are consistent with our previous work implicating Nrf2 pathway inhibition as a major driver of hyperinflammatory signatures in Polg mutant macrophages and mice[20]. We also observed that DMF reduced PA-induced cell death and hypersecretion of IL-1α and IL-1β in Polg mutant macrophages. By activating Nrf2 and/or inhibiting NF-κB, DMF reduces transcription of multiple pro-inflammatory cytokine genes including *Il1b*[55,56]. However, DMF can also directly impair NLRP3 activation and GSDMD-mediated pyroptosis[57,58], leading us to directly examine inflammasome activation in our Polg mutant models.

Our data reveal that Polg mutant macrophages have an increased propensity to undergo rapid pyroptosis upon PAO1 challenge in a caspase-1-dependent fashion. Although caspase-1 cleavage is elevated in Polg^{D257A} over WT macrophages during PAO1 challenge and its inhibition is sufficient to block augmented PA-induced cell death and IL-1β secretion, we found that Polg^{D257A} BMDMs are less responsive to direct activation of the NLRP3 and NLRC4 inflammasomes by their respective ligands. In contrast, activation of the non-canonical caspase-11 inflammasome via LPS priming followed by transfection of LPS into the cytosol drove more

PI uptake and IL-1β expression in Polg^{D257A} BMDMs. Caspase-11 expression is significantly elevated in Polg mutant BMDMs, collectively indicating that non-canonical inflammasome activation by cytosolic PA LPS leads to more robust activation of the NLRP3 inflammasome for caspase-1 dependent cell death and cytokine secretion. We hypothesize that increased caspase-11-dependent cleavage of GSDMD may lead to more rapid permeabilization of mitochondrial membranes in Polg mutant BMDMs, leading to augmented release of oxidized mtDNA or other mitochondrial DAMPs that potentiate activation of NLRP3[59–61]. It is also possible that potentiated release of mitochondrial RNA or mtDNA, or increased vita-PAMP accumulation in Polg BMDMs, may enhance caspase-11 and NLRP3 interaction, leading to elevated pyroptosis and pro-inflammatory cytokine secretion[62]. Finally, it is interesting to note that treatment of Polg mutant macrophages with caspase-1 inhibitor dramatically reduced most cytokine levels in culture supernatants after challenge with PAO1 (**Fig. 3f**). These included inflammasome-independent cytokines such as TNFα, IL-6, IFNγ, and IL-12 family members as well as the DAMP IL-1α, which does not require caspase-1 cleavage but is downstream of caspase-11 and GSDMD[37,63]. This is in contrast with cytokine secretion in WT BMDMs, where AcYVAD treatment only reduced IL-1β levels during challenge with PAO1. Overall, these data suggest key roles for caspase-11 and caspase-1 in the broad hyperinflammatory phenotype of Polg mutant mice.

We have also found that elevated IFN-I signaling is a key driver of caspase-11-dependent pyroptosis and hyperinflammation in Polg mutants. Inclusion of anti-IFNAR neutralizing antibodies was sufficient to reduce both augmented PI uptake after LPS transfection and cytokine hypersecretion after challenge with PAO1. Our prior work revealed that increased IFN-I signaling in Polg^{D257A} macrophages depends on chronic cGAS-STING signaling, and here we

show that Polg^{R292C} macrophages also exhibit increased expression of ISGs at rest and after challenge with PAO1[20]. Thus, alterations to IFN-I signaling appear to be a common feature in Polg mutant mice, human fibroblasts harboring the *POLG1* c.2243G>C, p.W748S variant[64], and peripheral blood mononuclear cells from patients with diverse MtD mutations[11]. IFN-I is critical to license caspase-11 expression[40], but also to enhance expression of interferon-inducible GTPases like GBPs, which help to expose cytosolic LPS for detection[34,65–68]. We have found that macrophages from both the Polg^{D257A} and our new MtD-relevant Polg^{R292C} macrophages exhibit enhanced expression of many GBPs at rest and after challenge with PAO1. Moreover, we observed that GBP5 strongly co-localizes to intracellular PAO1 in Polg mutant BMDMs, suggesting that IFN-I mediated triggering of GBPs potentiates LPS sensing by caspase-11 to augment cytokine secretion.

Although it is appreciated that bacterial and viral infections are problematic for the MtD population due to their propensity to trigger systemic hyperinflation and disseminated disease, few studies have examined immune responses in relevant mouse models of MtD. Using an intratracheal instillation model, we find that Polg^{D257A} mice exhibit hyperactive innate immune responses resulting in elevated cytokine production, changes in lung immune cell dynamics recruitment, and increased susceptibility to death following PAO1 infection. Notably, we observed elevated expression of inflammasome proteins, including caspase-11, ISGs including GBPs, and increased caspase-1 cleavage in Polg^{D257A} lung homogenates after infection. These data agree with our in vitro findings implicating IFN-I as an overarching regulator of caspase-1/11 activation and hyperinflammation in our models. Additional studies are warranted to define the cellular populations that govern lung hyperinflammation and to determine the degree to which caspase-11 shapes inflammatory signaling and morbidity in Polg mutant mice in vivo.

Overall, our study provides important new insight into the innate immune mechanisms governing infection-related hyperinflammation in mouse models Polg MtD and furthers our understanding of why patients with MtD are more prone to developing sepsis and SIRS following infection. DMF and/or other therapeutics targeting IFN-I and caspase-11 may therefore represent promising avenues to restore proper immune balance in the MtD population.

Figures and Legends

Fig. 1: Polg^{D257A} mutator macrophages exhibit increased IFN-I and pro-inflammatory responses after challenge with LPS or *Pseudomonas aeruginosa*.

(a) Workflow for preparing RNA from Polg BMDMs after *Pseudomonas aeruginosa* (PA) strain O1 (PAO1) challenge.

(b) Ingenuity Pathway Analysis (IPA) of RNA-seq from bone marrow-derived macrophages (BMDMs) showing Z-scores of pathways in Polg^{D257A} homozygous mutant BMDMs compared to wild-type (WT) after LPS, PAO1, or PAO1 plus dimethyl fumarate (DMF) challenge. hpc=hours post challenge. N=3 biological replicates/genotype/condition.

(c) Log^2 fold changes of representative genes in IPA pathways from (**b**) in Polg^{D257A} BMDMs compared to WT after LPS, PAO1, or PAO1 plus DMF.

(d) Protein abundance of interferon-stimulated genes (ISGs) in BMDMs exposed to PAO1 at a multiplicity of infection (MOI) of 5 at the indicated hours post challenge (hpc).

(e) Cytokines in supernatant of peritoneal macrophages (PerMacs) measured by ELISA. MOI= multiplicity of infection, N=3 biological replicates per time point.

(f) IPA Upstream Regulator analysis showing Z-scores in Polg^{D257A} homozygous mutant BMDMs compared to WT after LPS, PAO1, or PAO1 plus dimethyl fumarate (DMF) challenge.

(g) Log^2 fold changes Nrf2 target genes from IPA pathway (**b**) in $Polg^{D257A}$ BMDMs compared to WT after LPS, PAO1, or PAO1 plus DMF.

(h) qRT-PCR analysis of ISGs in WT and $Polg^{D257A}$ BMDMs after PAO1 or PAO1 plus DMF. N=3 biological replicates, 3 technical replicates/genotype/condition.

(i) Legendplex pro-inflammatory cytokines analysis of PerMac supernatants 24 hours post challenge (hpc). N=3 biological replicates

Statistics: (e, h, & i) Two-Way ANOVA. *P<0.05, **P<0.01, ***P<0.001, ****P<0.0001 Error bars represent SEM.

Fig. 2: $Polg^{D257A}$ mutant macrophages exhibit potentiated cell death upon PAO1 challenge.

(a) Ingenuity Pathway Analysis (IPA) of RNA-seq from bone marrow-derived macrophages (BMDMs) showing Z-scores of pathways related to cell death signaling in $Polg^{D257A}$ homozygous mutant BMDMs compared to wild-type (WT) after LPS, PAO1, or PAO1 plus dimethyl fumarate (DMF) challenge. hpc=hours post challenge. N=3 biological replicates/genotype/condition.

(b) Log^2 fold changes of representative genes in IPA pathways from **(a)** in $Polg^{D257A}$ BMDMs compared to WT after LPS, PAO1, or PAO1 plus DMF.

(c) Representative immunofluorescent (IF) images of peritoneal macrophages (PerMacs) after PAO1 or PAO1 plus DMF. Cells were stained with DAPI to mark the nucleus, CellMask to mark plasma membranes, and anti-GFP antibody to mark GFP-tagged PAO1. White arrows highlight dying cells characterized by condensed nuclei and loss of CellMask staining.

(d) Percent of PerMacs dying after PAO1 and PAO1 plus DMF in **(c)** IF. N= 5 IF images/genotype/condition.

(e) Cytation5 Image analysis of PI positive BMDMs after PAO1 or PAO1 plus DMF. N= 3 biological replicates, 5 technical replicates/genotype/condition.

(f) LegendPlex pro-inflammatory cytokines analysis of PerMac supernatants at 8 and 24 hpc in the presence or absence of DMF. N=3 biological replicates/genotype/condition.

Statistics: (e & f) Two Way ANOVA (d) One Way ANOVA. *P<0.05, **P<0.01, ***P<0.001, ****P<0.0001 Error bars represent SEM.

Fig. 3: Caspase-11 and caspase-1 drive pyroptosis and inflammation in Polg mutant macrophages challenged with PAO1.

(a) ELISA analysis of inflammatory cytokines in BMDM supernatant after PAO1 or PAO1 plus caspase inhibitors. N= 3 biological replicates/genotype/condition.

(b) Cytation5 image analysis of PI positive BMDMs after PAO1 or PAO1 plus caspase-1 inhibitor. N= 3 biological replicates, 5 technical replicates/genotype/condition.

(c) Percent PerMacs dying after PAO1 and PAO1 plus caspase-1 inhibitor from IF **(d)**. N=4 IF images/genotype/condition.

(d) Representative IF of PerMacs after PAO1 or PAO1 plus caspase inhibitor. Cells were stained with DAPI to mark the nucleus, CellMask to mark the total cell volume, and anti-GFP to mark GFP tagged PAO1. White arrows highlight dying cells characterized by condensed nuclei and loss of CellMask staining.

(e) Western blot analysis of lysates from BMDMs challenged with PAO1.

(f) LegendPlex pro-inflammatory cytokines analysis of BMDM supernatant 24 hpc. All undefined comparisons between WT and WT+AcYVAD are not significant. N=3 biological replicates/genotype/condition.

(g) Cytation5 image quantification of PI positive BMDMs after LPS priming plus LPS transfection and LPS priming plus LPS transfection plus caspase-1 inhibitor. N= 3 biological replicates, 5 technical replicates/genotype/condition.

(h) ELISA analysis of IL-1β in BMDM supernatant after LPS priming plus LPS transfection in the presence or absence of caspase-1 inhibitor. N=3 biological replicates

(i) qRT-PCR analysis of Caspase-11 RNA expression in BMDMs after PAO1. N=3 biological replicates, 3 technical replicates/genotype/condition.

(j) Cytation5 image quantification of PI positive cells in BMDMs after LPS priming plus LPS transfection and incubated with αIFNAR blocking antibody or αIgG control. N= 3 biological replicates, 5 technical replicates/genotype/condition.

Statistics: (c, f, & h) One-Way ANOVA (a, b, g, i & j) Two-Way ANOVA. *P<0.05, **P<0.01, ***P<0.001, ****P<0.0001 Error bars represent SEM.

Fig. 4: Increased GBP expression and targeting to intracellular PAO1 in Polg^{D257A} macrophages.

(a) RNA-seq from BMDMs showing induction of Gbps and Caspase-11 RNA 6 hours post challenge (hpc) with PAO1. N=3 biological replicates/genotype/condition.

(b) Representative IF of unchallenged BMDMs stained with DAPI to mark the nucleus and anti-GBP5 antibody.

(c) Sum intensity of GBP5 per cell area in resting BMDMs in (**b**) IF. N=7 images/genotype

(d) Representative IF of BMDMs 2 hpc with PAO1 at a multiplicity of infection (MOI) of 5. Cells were fixed, permeabilized, and stained with DAPI to mark the nucleus, anti-LPS antibody to stain PAO1 LPS, and anti-GBP5 antibody.

(f) Sum intensity of GBP5 per cell area in BMDMs after PAO1 in **(d)** IF. N=7 images/genotype.

(e) Sum intensity of PAO1-LPS localized with GBP5 in BMDMs after PAO1 in **(d)** IF. N=7 images/genotype.

Statistics: (a, c, e, & f) Student's t-test. *P<0.05, **P<0.01, ***P<0.001, ****P<0.0001 Error bars represent SEM.

Fig. 5: Macrophages incorporating a deleterious patient mutation (Polg^{R292C}) exhibit mtDNA depletion, elevated IFN-I responses, increased pyroptosis, and hyper-inflammation after challenge with PAO1

(a) Generation of the Polg^{R292C} mouse.

(b) Chromatograph from Sanger sequencing of DNA from heterozygous Polg^{R292C} mouse verifying germline incorporation of mutation.

(c) qPCR analysis of mtDNA abundance in BMDMs. N= 3 biological replicates, 3 technical triplicates/genotype.

(d) Representative IF of nucleoids in BMDMs stained with anti-PDH antibody to label mitochondria, anti-DNA antibody to label nucleoids, and anti-TFAM antibody.

(e) Quantification of nucleoids per cell, mean intensity of DNA signal per nucleoid, and nucleoid area per cell from BMDMs in **(d)** IF. N=40-50 cells/genotype

(f) qRT-PCR analysis of ISGs in BMDMs after PAO1, N=3 biological replicates, 3 technical replicates/genotype.

(g) Representative IF of BMDMs after PAO1 stained with DAPI to mark the nucleus, CellMask to mark the total cell volume, and anti-GFP to mark GFP tagged PAO1. White arrows highlight dying cells characterized by condensed nuclei and loss of CellMask staining.

(h) Percent BMDMs dying after PAO1 in **(g)** IF. N=7 IF images/genotype.

(i) ELISA analysis of inflammatory cytokines in BMDM supernatant after PAO1. N= 3 biological replicates.

Statistics: (c, e, f, & h) Students t-test. (i) Two-Way ANOVA. *P<0.05, **P<0.01, ***P<0.001, ****P<0.0001 Error bars represent SEM.

Fig. 6: Intratracheal instillation of PAO1 into lungs elicits greater inflammation, caspase-11 expression, and death of Polg mutant mice.

(a) LegendPlex pro-inflammatory cytokine analysis of bronchial alveolar lavage (BAL) 6 hours post infection (hpi) with $1x10^4$ colony forming units (CFU) of PAO1. N=5 mice/genotype

(b) Protein expression or WT and $Polg^{D257A}$ lung homogenates 48 hpi with $1x10^4$ CFU of PAO1.

(c) Representative hematoxylin and eosin (H&E) staining of lung sections 20 hpi with $1x10^5$ CFU of PAO1.

(d) Pathology scoring of lung sections from **(c)**.

(e) Graphs of pathology scoring from H&E stained lungs in **(d)** histology. N=5 mice/genotype

(f) Protein expression or WT and $Polg^{D257A}$ lung homogenates 20 hpi with $1x10^5$ CFU of PAO1.

(g) Kaplan-Meier survival curve after infection with $1x10^5$ CFU of PAO1. N= 7 mice/genotype

(h) Graphical abstract depicting findings of the study.

Statistics: (a & e) Students t-test (g) Kaplan-Meijer Survival Curve. *P<0.05, **P<0.01, ***P<0.001, ****P<0.0001 Error bars represent SEM.

Supplementary Fig. 1: $Polg^{D257A}$ macrophages exhibit elevated IFN-I and pro-inflammatory gene expression when challenged with LPS or PAO1.

(a) Log^2 fold changes of representative genes in IPA pathways from (**Fig. 1b**) in $Polg^{D257A}$ BMDMs compared to WT after challenge with LPS, PAO1, or PAO1 plus DMF. N=3 biological replicates/genotype/condition.

(b) Gene Set Enrichment (GSEA) pathways of RNA-seq data in WT ang $Polg^{D257A}$ BMDMs after challenge with PAO1 and PAO1 plus DMF. Heatmaps represent fold changes of each group relative to WT PAO1 infected. N=3 biological replicates/genotype/condition.

Supplementary Fig. 2: $Polg^{D257A}$ macrophages exhibit increased inflammatory cell death when exposed to bacteria.

(a) Representative IF of BMDMs unchallenged or primed with LPS for 4 hours and stimulated with nigericin for 1 hour to activate the NLRP3 inflammasome. Cells are stained with DAPI to mark the nucleus, CellMask to mark total cell volume, and anti-ASC antibody to mark puncta.

(b) Number of ASC puncta per cell in cells with high and low CellMask staining in **(a)** IF. N= 7 images/condition.

(c) PAO1 colony forming units obtained from BMDM supernatant or detergent lysates 2 and 4 hours post challenge (hpc). N=4 biological replicates.

(d) Beads per cell quantified from **(e)** IF. N= 100 cells/genotype.

(e) Representative IF of BMDMs phagocytosing LPS coated, fluorescent microspheres. Cells were stained with DAPI to mark the nucleus, CellMask to label the cell volume, and anti-LAMP1 to mark phagolysosomes.

(f) ELISA analysis of inflammatory cytokines in BMDM supernatants after challenge with *Escherichia coli* strain DH5α. N= 3 biological replicates.

(g) Percent BMDMs dying after challenge with DH5α **(h)** IF. N=7 IF images/genotype.

(h) Representative IF of BMDMs stained with DAPI to mark the nucleus, CellMask to mark the total cell volume, and anti-LPS to mark DH5α bacteria. White arrows highlight dying cells characterized by condensed nuclei and loss of CellMask staining.

Statistics: (c & f) Two-way ANOVA (b, d, & g) Students t-test. *P<0.05, **P<0.01, ***P<0.001, ****P<0.0001 Error bars represent SEM.

Supplementary Fig. 3: Assessment of roles for canonical inflammasome activity, metabolism, and IFN-I dependence in driving increased cell death and pro-inflammatory cytokine secretion in Polg mutant macrophages.

(a) Cytation5 imaging quantification of PI positive cells in BMDMs after LPS priming for 4 hours. N= 3 biological replicates, 5 technical replicates/genotype.

(b) Cytation5 imaging quantification of PI positive cells in BMDMs after LPS priming plus PA-flagellin transfection. N= 3 biological replicates, 5 technical replicates/genotype.

(c) ELISA analysis of IL-1β in BMDM supernatant after LPS priming plus PA-flagellin transfection. N= 3 biological replicates.

(d) Cytation5 imaging quantification of PI positive cells in BMDMs after LPS priming plus ATP. N= 3 biological replicates, 5 technical replicates/genotype.

(e) ELISA analysis of IL-1β in BMDM supernatant after LPS priming plus ATP. N= 3 biological replicates.

(f) Western blot of BMDM protein lysates after LPS priming plus ATP.

(g) Cytation5 imaging quantification of PI positive cells in BMDMs after LPS priming plus nigericin. N= 3 biological replicates, 5 technical replicates/genotype.

(h) ELISA analysis of IL-1β in BMDM supernatant after LPS priming plus nigericin. N= 3 biological replicates.

(i) Western blot of BMDM protein lysates after LPS priming plus nigericin.

(j) & **(k)** Seahorse analysis of BMDMs unchallenged or treated with overnight LPS. Extracellular acidification rate (ECAR) **(j)** and oxygen consumption rate (OCR) **(k)** are plotted. N=3 biological replicates and 5 technical replicates.

(l) Quantification of Seahorse OCR measurements. N=3 biological replicates and 5 technical replicates.

(m) ELISA analysis of inflammatory cytokines in BMDM supernatant after PAO1 challenge in the presence of αIFNAR neutralizing antibody or αIgG. N= 3 biological replicates.

Statistics: (b, e, & h) Two-Way ANOVA (l & m) One-Way ANOVA (a, c, f, & i) Students t-test. *P<0.05, **P<0.01, ***P<0.001, ****P<0.0001 Error bars represent SEM.

Supplementary Fig. 4: Polg mutant mice exhibit elevated IFN-I and inflammatory responses to LPS, but do not exhibit basal differences in lung morphology or immune cell abundance.

(a) qRT-PCR analysis of ISGs in unchallenged $Polg^{R292C}$ BMDMs. N=3 biological replicates, 3 technical replicates/genotype.

(b) qRT-PCR analysis of ISGs in $Polg^{R292C}$ BMDMs 8 hours post challenge (hpc) with LPS. N=3 biological replicates, 3 technical replicates/genotype.

(c) Representative histology images of hematoxylin and eosin (H&E) staining of WT and $Polg^{D257A}$ lungs, with an overlay of eosin positive cells using QuPath software.

(d) Pathology assessment of unchallenged lungs.

(e) QuPath analysis of $eosin^{+}$ cells in the lungs from **(c)**. N=3 mice/genotype

(f) Protein expression of ISGs in unchallenged WT and $Polg^{D257A}$ lungs homogenates.

(g) ELISA analysis of inflammatory cytokines in bronchioalveolar lavage of LPS challenged WT and $Polg^{D257A}$ lungs. N=2 mice/genotype/timepoint.

Statistics: (g) Two-Way ANOVA (a, b, & e) Students t-test. *P<0.05, **P<0.01, ***P<0.001, ****P<0.0001 Error bars represent SEM.

Supplementary Fig. 5: Intratracheal instillation of PAO1 alters immune cell composition in Polg mutant mouse lungs.

(a) Weight change in WT and $Polg^{D257A}$ mice after infection with $1x10^4$ PAO1. N=5 mice/genotype.

(b) CD45 expression on cells from bronchioalveolar lavage (BAL) from uninfected and PAO1 infected WT and $Polg^{D257A}$ mice. N=5-9 mice/genotype/timepoint.

(c) Gates used to quantify CD45 expression in **(b)**.

(d) Percent of $CD45^+$ cells expressing CD11c from the BAL of uninfected and PAO1 infected lungs. N=5-9 mice/genotype/timepoint.

(e) Percent of $CD45^+$ cells expressing SiglecF from the BAL of uninfected and PAO1 infected lungs. N=5-9 mice/genotype/timepoint.

(f) Percent of $CD45^+$ cells expressing MHCII from the BAL of uninfected and PAO1 infected lungs. N=5-9 mice/genotype/timepoint.

(g) Percent of $CD45^+$ cells expressing F4/80 from the BAL of uninfected and PAO1 infected lungs. N=5-9 mice/genotype/timepoint.

(h) Percent of $CD45^+$ cells expressing CD11b from the BAL of uninfected and PAO1 infected lungs. N=5-9 mice/genotype/timepoint.

(i) Percent of $CD45^+$, $CD11b^-$ cells expressing CD3 from the BAL of uninfected and PAO1 infected lungs. N=5-9 mice/genotype/timepoint.

(j) Percent of $CD45^+$, $CD11b^-$ cells expressing CD19 from the BAL of uninfected and PAO1 infected lungs. N=5-9 mice/genotype/timepoint

(k) Percent of $CD45^+$ expressing Ly6G from the BAL of uninfected and PAO1 infected lungs. N=5-9 mice/genotype/timepoint.

(l) Percent of $CD45^+$ cells expressing Ly6C from the BAL of uninfected and PAO1 infected lungs. N=5-9 mice/genotype/timepoint.

(m) $CD45^+$ cells with cell associated TNFα expression from BAL of uninfected and PAO1 infected lungs. N=5-9 mice/genotype/timepoint.

Statistics: (a) Two-way ANOVA (b, & d-m) Students t-test. *P<0.05, **P<0.01, ***P<0.001, ****P<0.0001 Error bars represent SEM.

Supplementary Fig. 6: Polg mutant mice exhibit hyperinflammation in response to infection and reinfection with PAO1.

(a) LegendPlex pro-inflammatory cytokine analysis of bronchioalveolar lavage (BAL) from WT, $Polg^{D257A}$, WT $IFNAR^{-/-}$, and $Polg^{D257A}$ $IFNAR^{-/-}$ lungs infected with $1x10^4$ PAO1 for 48 hours. All undefined comparisons are not significant. N=5 mice/genotype.

(b) Representative histology images of hematoxylin and eosin (H&E) staining of WT and $Polg^{D257A}$ lungs after initial infection with $1x10^4$ PAO1, followed by 7 days rest, then reinfection with $1x10^4$ PAO1. Overlay of eosin positive cells was done using QuPath software.

(c) QuPath analysis of $eosin^+$ cells in the lung from **(b)** histology. N=5 mice/genotype.

(d) LegendPlex pro-inflammatory cytokine analysis of BAL from WT and $Polg^{D257A}$ lungs after initial infection with $1x10^4$ PAO1, followed by 7 days rest, then reinfection with $1x10^4$ PAO1. N=5-6 mice/genotype.

(e) Colony counts from homogenized tissue after initial infection with $1x10^4$ PAO1, followed by 7 days rest, then reinfection with $1x10^4$ PAO1. N=5 mice/genotype.

(f) Colony counts from homogenized tissue infected with $1x10^5$ PAO1. N=5 mice/genotype.

Statistics: (a) Two-way ANOVA (c, d, e, & f) Students t-test. *P<0.05, **P<0.01, ***P<0.001, ****P<0.0001. Error bars represent SEM.

Acknowledgements

We thank R. Moore at the Texas A&M School of Medicine Analytical Cytometry Core for flow cytometry assistance.

Funding

This research was supported by awards W81XWH-17-1-0052 to A.P.W. and W81XWH-20-1-0150 to C.C. and A.P.W. from the Office of the Assistant Secretary of Defense and for Health Affairs through the Peer Reviewed Medical Research Programs. Additional support was provided by NIH grants R01HL148153 to A.P.W., U54OD030187 to S.A.M, and a gift from the POLG Foundation. J.J.V. was supported by NIH NRSA F31AI179168 and Y. Lei was supported by American Heart Association Predoctoral Fellowship grant 825908.

Author contributions

A.P.W and J.J.V. designed experiments, analyzed data, and wrote the manuscript. Y.L. assisted with animal experiments and sample processing. C.G.M. performed inflammasome challenge experiments. J.W. assisted with pathology scoring of histology samples. C.P. and R.S. maintained animals and generated macrophages. S.C.K. and S.A.M. generated the $Polg^{R292C}$

mouse model and provided samples. P.J.M. and C.L.C. assisted with data analysis and interpretation. A.P.W. conceived the project and provided overall direction.

Competing interests

The authors declare that they have no competing interests.

Data and materials availability

All data needed to evaluate the conclusions drawn herein are present in the paper and Supplementary Materials. Raw data will be provided upon request. The RNA sequencing datasets generated through this work will be deposited in the Gene Expression Omnibus after acceptance of the paper for publication.

Methods

Mouse Husbandry and Strains

C57BL/6J (JAX Stock # 000664), Polg$^{D257A/D257A}$ (JAX Stock # 017341), and *Ifnar1*$^{-/-}$ (JAX Stock # 028256) mice were obtained from The Jackson Laboratory and bred and maintained in multiple vivaria at Texas A&M University and The Jackson Laboratory. Experimental Polg$^{+/+}$ and Polg$^{D257A/D257A}$ littermates were obtained from Polg$^{D257A/+}$ maintenance colony crosses of male Polg$^{D257A/+}$ to female Polg$^{+/+}$. This breeding strategy was adopted to limit the accumulation and maternal transmission of mutant mtDNA molecules to heterozygous breeders.

The Polg$^{R292C/R292C}$ mouse line (B6N(Cg)-Polgem5(F290F,R292C)Lutzy/Mmjax) was generated using CRISPR/Cas9 endonuclease-mediated genome editing in mouse embryonic stem

cells (mESCs). A single guide RNA (CTCCCATCCACAGGCTGCGC) targeting exon 4 of Polg was cloned into pX459, which expresses Cas9 nuclease. This plasmid was co-delivered to JM8A3 ESCs via electroporation with a single-stranded oligonucleotide donor (ssODN) that included the missense R292C (CGC>TGC) and an additional silent mutation (F290F; TTC>TTT) to reduce recutting of the targeted allele. Following puromycin selection, resistant clones were screened for proper targeting and to exclude integration of the pX459 plasmid. Multiple clones were selected for expansion and karyotyping, and euploid clones were injected into C57BL/6J-albino blastocysts (B6(Cg)-Tyrc-2J/J; JAX STOCK# 000058) to produce chimeras. Chimeras were bred to C57BL/6NJ (JAX Stock #005304) mice and a single germline clone was selected for expansion and characterization. The line is available through the MMRRC repository (071656-JAX).

All animal experiments were approved by the Institutional Animal care and Use Committees (IACUC) at Texas A&M University and The Jackson Laboratory.

Cell Culture

L929 cells were obtained from ATCC and maintained in DMEM (Sigma-Aldrich, D5796) and 10% fetal bovine serum (FBS; VWR, 97068-085). Primary bone marrow-derived macrophages (BMDMs) were isolated from femurs of 6-12 month old WT, $Polg^{D257A}$ and 2-6 month old $Polg^{R292C}$ mice as described[20]. Briefly, whole femurs were crushed in media and passed through a 70 µm filter. Red blood cells were lysed through osmosis by resuspending in ACK lysis buffer (Quality Biological, 118-156-101) for 2 minutes. Remaining cells were passed through a 40 µm filter, counted, and plated on non-tissue culture treated dishes. Macrophages were differentiated over for 7 days using 30% L929 conditioned medium. Peritoneal

macrophages (PerMacs) were collected from the peritoneal cavity via gavage 4 days after intraperitoneal injection of 3% brewer thioglycolate medium (Sigma-Aldrich, B2551) and plated in in medium with 10% FBS. Unless stated, 6 x 10^5 BMDMs and $1.2x10^6$ PerMacs per millimeter were used in in vitro experiments. Cells were plated and left to adhere overnight prior to challenge.

***Pseudomonas aeruginosa* (PAO1) in vitro infection**

GFP expressing PAO1 was provided by the Cannon laboratory and was grown on Soy agar plates (BD, 211043) with 100 µg/mL carbenicillin (Dot Scientific, 46000-5) overnight from a glycerol stock. A single colony was incubated in 5 mL Mueller Hinton broth (BD, 275730) with carbenicillin at 37 □C spinning overnight. Overnight culture was back diluted 1:5 and grown for 2 hours until bacteria reached log-phase. Bacteria were washed with sterile phosphate-buffered saline (PBS) and opsonized for 20 minutes in mouse serum (Fisher, PI31880). After two more washed with PBS macrophages were infected at the corresponding MOI and spun at 250 g for 5 minutes to synchronize infection. For inhibitor experiments, cells were primed with 10 µM Ac-YVAD-cmk (Invivogen, inh-yvad) or 10 uM Q-VD-OPh (Millipore Sigma, 551476) for 3 hours prior to challenge. One hour after infection, wells were washed and treated with 300 µg/mL gentamicin (VWR, 0304) for 30 minutes to inactivate extracellular bacteria. The rest of the experiment was completed in media supplemented with 50 µg/mL gentamicin and 50 µM dimethyl fumarate (DMF; Sigma-Aldrich, 242926) or inhibitor when described.

RNA sequencing and bioinformatic analysis

Total cellular RNA was prepared from uninfected BMDMs, infected BMDMs, and infected BMDMs treated with 50 μM DMF using Quick-RNA microprep kit (Zymo Research, R1051) and used for the next-generation RNA-sequencing procedure at Texas A&M University Bioinformatics Core. BaseSpace Sequence Hub (Illumina) was used for RNA seq analysis. Briefly, Spliced Transcripts Alignment to a Reference (STAR) algorithm of RNA-seq Alignment V2.0.0 software was used to align the results to reference genome Mus musculus/mm10 (RefSeq), and then RNA-seq Differential Expression V1.0.0 software was used to obtain raw gene expression files and determine statistically significant changes in gene expression in Polg macrophages relative to WT. Ingenuity Pathway Analysis software (QIAGEN) was used to identify gene families and putative upstream regulators in the datasets. Gene Set Enrichment Analysis (GSEA) Software (Broad Institute) was used to generate enrichment plots and examine pathway enrichment. Heatmaps were generated using GraphPad Prism. Datasets of LPS-treated $Polg^{D247A}$ BMDMs used in Fig. 1-2 and Supplementary Fig. 1 were previously reported[20] and are available under Gene Expression Omnibus number GSE171960. Raw gene counts from PAO1-infected $Polg^{D247A}$ BMDMs are supplied for review in a supplemental data spreadsheet. These data will be deposited into the Gene Expression Omnibus upon acceptance of the paper for publication.

***Escherichia coli* (E. coli) in vitro infection**

E. Coli containing empty pcDNA3.1 vector for antibiotic resistance was grown on LB agar plates (Fisher, DF0401-17) with 100 μg/mL carbenicillin (Dot Scientific, 46000-5) overnight from a glycerol stock. A single colony was incubated in 5 mL LB broth (Fisher, BP1427-500) with carbenicillin at 37 □C spinning overnight. Overnight culture was back diluted

1:5 and grown for 2 hours until bacteria reached log-phase. Bacteria were washed with sterile phosphate-buffered saline (PBS) and opsonized for 20 minutes in mouse serum. After two more washed with PBS macrophages were infected at the corresponding MOI and spun at 250 g for 5 minutes to synchronize infection. One hour after infection, wells were washed and treated with 300 μg/mL gentamicin (VWR, 0304) for 30 minutes to kill extracellular bacteria. The rest of the experiment was completed in DMEM + 10% FBS supplemented with 50 μg/mL gentamicin.

Inflammasome challenge

BMDMs were primed for 4 hours with 20 ng/mL LPS-B5 Ultrapure (InvivoGen, tlrl-pb5lps). When used, caspase inhibitor Ac-YVAD-cmk (InvivoGen, inh-yvad) was added an hour after LPS, to allow for 3 hour priming, at 10 μM concentration. To trigger the non-canonical and NLRC4 inflammasomes respectively, polyethyleneimine (Alfa Aesar, 43896) was used to transfect 2 μg/mL LPS[69] and 100 μg/mL PA flagella[70] into the cytosol. To trigger the NLRP3 inflammasome, 5 μM ATP (Sigma, A6419) or 40 μM Nigericin (Cayman Chemical Company, 11437) was added to the media. When used, 20 μg/mL anti-IFNAR antibody (Bio X Cell, BE0241) or anti-IgG control (Bio X Cell, BE0083) were added to cells 5 hours prior to LPS priming and added again upon LPS transfection.

Immunoblotting

Cells and tissues were lysed in 1% NP-40 lysis buffer supplemented with protease inhibitor and then centrifuged at 15,000 rpm for 10 min at 4 □C and the supernatant was collected as the cellular lysate. A bicinchoninic acid assay (BCA) protein assay (Thermo Fisher Scientific, PI23235), was used to quantify protein and 10 to 40 μg total protein were loaded into

10% SDS-polyacrylamide gels and transferred onto 0.22 μM polyvinylidene difluoride membranes. Membranes were dried to return them to a hydrophobic state and then incubated in primary antibodies diluted in 1x PBS containing 1% casein overnight at 4 □C rolling. Membranes were washed and incubated with horseradish peroxidase (HRP)- conjugated secondary antibodies for 1 hour at room temperature, shaking. Membranes were developed with Luminata Crescendo Western HRP Substrate (Millipore, WBWR0500). Primary antibody information can be found in Table 1.

LegendPlex multianalyte cytokine analysis

Supernatants from macrophages were subjected to centrifugation prior to the assay to remove detached cells and debris from the sample. The assay was completed using the LegendPlex Mouse Inflammation Panel (BioLegend, 740446) according to the included protocol. Samples were analyzed by flow cytometry using a 5L Cytek Aurora and the BioLegend analysis software. Samples were normalized to total protein content of each sample determined by a bicinchoninic acid assay (BCA) protein assay and MFI from the blank control beads was subtracted to exclude background.

Enzyme-linked immunosorbent assay (ELISA)

Supernatants were collected from macrophages plated on glass coverslips. Macrophages were stained for IF analysis while supernatants were subjected to centrifugation to remove detached cells and debris from the sample. Samples were stored at -80C until use in this assay and were thawed on ice upon use. The assay was completed in 96-well half area clear, flat bottom plates (USA Scientific, 5667-5061) and wells were incubated overnight at 4□C in

capture antibodies. Blocking was completed for one hour with PBS containing 10% FBS at room temperature. Standards and samples were added to wells for two hours. All sample dilutions were made in blocking buffer. Next, wells were incubated in detection antibody for one hour. Avidin-HRP and trimethyl boron (TMB) were used for quick color development. Plates were washed with PBS containing 0.05% Tween 20 between each step. Capture and detection antibodies were used in the following pairs from BioLegend: Il-1β (Cat # 503514, 515801); TNFα (Cat # 506310, 506312) and IL-6 (Cat # 504501, 504601). Samples were normalized to corresponding nuclei counts from 20X IF images taken on an EDLIPSE Ti2 (Nikon). Nuclei counts were determined using the automated bright spot counting function in NIS-Elements on DAPI and an average of 3 images was used to normalize ELISA. ELISA concentrations were determined using an epoch plate reader (BioTek) and BioTek Gen5 software. Normalized results were graphed in GraphPad.

Quantitative polymerase chain reaction

Relative gene expression with measured by qRT-PCR in cells. Total cellular RNA was isolated using Quick-RNA microprep kit (Zymo Research, R1051). Approximately 0.5 µg of RNA was used to make cDNA with XLT qScript cDNA Synthesis Kit (Quantabio, 95047). cDNA was then used in a qPCR assay using PerfeCTa Green FastMix (Quantabio, 95071). Two to three biological replicates and two to three technical replicates were normalized to *Rpl37* cDNA using the $2^{-\Delta\Delta CT}$ method. All primer sequences can be found in Table 2.

Immunofluorescence (IF) imaging

Cells were seeded at $2.5x10^5$ cell/well in a 24 well plate and allowed to grow overnight on glass coverslips sterilized with ethanol. After challenge or infection, cells were washed in PBS and fixed with 4% paraformaldehyde for 20 minutes. Next cells were permeabilized with 0.1% Triton X-100 in PBS for 5 minutes, blocked with PBS containing 5% FBS for 30 minutes, stained with primary antibodies for 1 hour, stained with secondary antibodies for 1 hour, and stained with 200 ng/mL 4',6-diamidino-2-phenylindole (DAPI) (ThermoFisher Scientific, 62247) for 2 minutes. When described, coverslips were stained with 2 µg/mL CellMask (Thermo Fisher Scientific, C10046) for 10 minutes after secondary antibody staining and washed multiple times in PBS before DAPI staining. Coverslips were mounted with ProLong Diamond Antifade Mountant (Invitrogen, MP33025) and sealed with nail polish. Cells were imaged with a 40x or 60x oil-immersed objective with an ECLIPSE Ti2 widefield microscope (Nikon) and analyzed with the NIS-Elements AR 5.21.02 software.

Quantification was done from multiple intensity projection (MIP) images generated from Z-stacks. MIPs were made and analysis was done using NIS-Elements AR 5.21.02. Specifically, cell death was determined using the automated bright spot counting function in NIS-Elements on DAPI to count the number of nuclei. Dying cells were manually determined by identifying cells with condensed nuclei and low CellMask staining. Percentage of dying cells were determined and graphed in GraphPad. To quantify nucleoids, whole cells were outlines and made into a region of interest (ROI) and these ROIs were numbered. A thresholding mask was made on the channels with TFAM and DNA staining and channel intensities were determined for these masks and graphed. A new mask was made based on the overlap of TFAM and DNA. The area of this mask and number of spots per ROI were exported and graphed in GraphPad. For GBP quantification, cells were counted using the automated bright spot counting function in NIS-

Elements on DAPI. A thresholding mask was made on GBP5 and LAMP1 and total intensities of each of these channels were exported. Next, a new mask was made for the overlap of these channels and the intensity of each channel in this mask was exported and graphed. Graphs and statistics were generated in GraphPad. Huygens Essential software (v21.4.0) was used to deconvolve representative images from z-stacks taken with a 60X objective in oil immersion.

PI uptake

BMDMs in 96 well half area glass bottom imaging plates were seeded at $6x10^4$ cells/well in 50 µL of Phenol-Red free DMEM + 10% FBS. The next day, cells were subjected to inflammasome challenge or infection with PAO1. Propidium iodide (PI, Alfa Aesar, J66584) was added to media and plates were immediately imaged every ten minutes using a BioTek Cytation V imager_which maintains 37 □C and 5% CO_2. PI positive nuclei were identified and counted using BioTek Gen5 software. Control wells treated with PI and Triton X-100 (to permeabilize cells) to for normalization. The difference between PI positive cells compared to the initial reading were graphed in line graphs using GraphPad Prism.

mtDNA copy number analysis

DNA was isolated from cells by boiling for 30 minutes in 50 mM NaOH lysis buffer and then neutralizing using 1 M Tris, pH8 solution. DNA was diluted to 2 ng/uL and utilized in qRT-PCR reaction (described above) with mtDNA specific primers. Two to three biological replicates and two to three technical replicates were normalized to nuclear encoded *Tert* using the $2^{-\Delta\Delta CT}$ method. All primer sequences can be found in Table 3.

In vivo PAO1 infection

6-7 month old mice were moved into BSL2 procedure space and allowed to acclimate for 1-2 days. Mice were anesthetized with an intraperitoneal injection of 100-10 mg/kg Ketamine-Xylazine cocktail. Mice were then intubated with a 24G catheter. Sterile PBS (sham), 0.5 mg/kg LPS (E. Coli serotype 0111:B4; Invivogen), or the specified dose of PAO1-GFP was pipetted into the catheter in a 25-30 µL volume. A bolus of air was delivered using a syringe to ensure the dose evenly coated the lungs. Mice were kept warm until fully recovered from anesthesia and monitored daily until experimental timepoints were reached.

Bronchial alveolar lavage fluid collection

Mice were euthanized using intraperitoneal injection of 200 mg/kg Pentobarbital Sodium to preserve the lung environment and structure of the tracheal. Upon confirmation of death the chest cavity and throat were opened. The trachea was canulated using a 23G needle threaded with tubing and the lung was washed with 3mL cold Hanks' Balanced Salt Solution (HBSS, Thermo Fisher Scientific, 14175-129) containing 100 µM EDTA (VMR Life Science, E522) and used in subsequent flow cytometry and LegendPlex assays.

Flow Cytometry

Bronchial alveolar lavage fluid (BAL) was spun at 350 g for 5 minutes to pellet the cells. Cells were transferred to a v bottom plate for staining. Cells were stained with viability dye then Fc receptors were blocked with anti-mouse CD16/CD32 (2.4G2) antibody. Surface proteins were stained with antibodies specified in Table 4. Cells were permeabilized with Foxp3/Transcription

Factor Staining Buffer Kit (TNB-0607-KIT, Tonbo) and stained with antibodies against intracellular proteins. Flow cytometry analysis was done using a 5L Cytek Aurora.

Colony forming unit counts from macrophages and tissues

BMDMs or tissues were homogenized in 0.1% NP40 in sterile PBS using an immersion homogenizer for 15 seconds per tissue. Serial dilutions were plated on soy agar containing 100 μg/mL carbenicillin. Plates were incubated at 37°C overnight and colonies were counted.

Histology

Tissues were collected in cassettes, then were washed in PBS, incubated for 24 hours in 10% formalin, and transferred to 70% ethanol. Tissue embedding, sectioning, and staining were performed at AML Laboratories in Jacksonville, FL or at the histology core at Texas A&M University. Images of hematoxylin and eosin (H&E) staining were collected using an Olympus slide scanner with a 20X objective. Slides were analyzed and scored by a pathologist, Dr. Jessica Wong, at the Jackson Laboratory in Sacramento, CA.

Statistical Analyses

To ensure rigor and reproducibility, experiments were repeated at least three times with multiple biological replicates. Error bars displayed throughout the manuscript represent the mean +/- s.e.m. Statistical significance between 2 groups was determined via unpaired, two-tailed Student's t-test or Mann-Whitney test, and differences between 3 or more groups was determined by two-way ANOVA with appropriate post-test. Survival plots were compared by the Log-rank test. Sample sizes were chosen by started methods to ensure adequate power, and no

randomization or blinding was used for animal studies. Significance was established as * $p<0.05$; ** $p<0.01$; *** $p<0.001$; **** $p<0.0001$; or not significant (ns).

Tables:

Table 1: Western blot antibodies

Protein	Company	Catalog
IFIT3	Ganes Sen, Cleveland Clinic	N/A
STAT1	Cell Signaling Technology	9172
GAPDH	ProteinTech	60004-1-Ig
HSP60	Santa Cruz Biotechnology	Sc-1052
CASPASE-11	Cell Signaling Technology	14340
GSDMD	Abcam	ab209845
NLRP3	Cell Signaling Technology	15101
CASPASE-1	Adipogen	AG-20B0042-C100
ZBP1	Adipogen	AG-20B-0010
IL-1β	Cell Signaling Technology	12242
NLRC4	Abcam	Ab201792
GBP5	Cell Signaling Technology	67798

Table 2: Primer sequences for qRT-PCR analysis

Gene	F Primer 5'→ 3'	R Primer 5'→ 3'
Cxcl10	CCAAGTGCTGCCGTCATTTTC	GGCTCGCAGGGATGATTTCAA
Ifit1	CAAGGCAGGTTTCTGAGGAG	GACCTGGTCACCATCAGCAT
Casp11	TGTCATCTCTTTGATATATTCCTGAAG	CAAGGTTGCCCGATCAAT
Gbp2	CAGCATAGGAACCATCAACCA	TCTACCCCACTCTGGTCA
Gbp4	CAGGCTCTACATGGACATGAGG	TGCCTGCAAGATGGAACTCTCG
Gbp9	TCGTGGCTATTGTTGGATTG	GGTCTGAGACTGCACAGTGGG
Rpl37	CATCCTTTGGTAAGCGTCGCA	TGGCACTCCAGTTATACTTCCT
Stat1	CGCGCATGCAACTGGCATATAACT	ATGCTTCCGTTCCCACGTAGACTT
Zbp1	TCAAAGGGTGAAGACATGACAGAC	GTGGGTGGCTTCAGAGCTT

Table 3: Primers for mtDNA copy number analysis by qPCR

Gene	F Primer 5'→ 3'	R Primer 5'→ 3'
mt Non-	CTAGAAACCCCGAAACCAA	CCAGCTATCACCAAGCTCGT

numpt		
mt D-loop	AATCTACCATCCTCCGTGAAACC	TCAGTTTAGCTACCCCCAAGTTTAA
mt Cytb	GCTTTCCACTTCATCTTACCATTTA	TGTTGGGTTGTTTGATCCTG
nuc tert	CTAGCTCATGTGTCAAGACCCTCTT	GCCAGCACGTTTCTCTCGTT

Table 4: Flow cytometry antibody panel

Antigen	Fluorophore	Laser	Company	Catalog/ Ref #
CD45	BUV395	UV2	BD	564279
Ly6C	BV650	V11	BioLegend	128049
MHCII	BV711	V13	BioLegend	107643
CD19	BV605	V10	BioLegend	115539
CD3	APC-fire810	R8	BioLegend	100267
F4/80	VF450	V3	TONBO Biosciences	75-4801-U025
PA01	FITC	B2		
CD11c	PE-Cy5	YG5	TONBO Biosciences	55-0114-U100
TNF	PE-Cy7	YG9	Biolegend	506324
Ly6G	PE	YG1	TONBO Biosciences	50-1276-U100
Siglec-F	APC	R1	Biolegend	155508
CD11b (M1/70)	APC-Cy7	R7	TONBO Biosciences	25-0112-U100
CD326	PE/Dazzel 594	YG3	Biolegend	118235
Viability	Ghost Dye 710	R4	TONBO Biosciences	13-0871-T100

References

1. Gorman, G. S. *et al.* Mitochondrial diseases. *Nat. Rev. Dis. Primer* **2**, 16080 (2016).
2. Suomalainen, A. & Battersby, B. J. Mitochondrial diseases: the contribution of organelle stress responses to pathology. *Nat. Rev. Mol. Cell Biol.* **19**, 77–92 (2018).
3. Russell, O. M., Gorman, G. S., Lightowlers, R. N. & Turnbull, D. M. Mitochondrial Diseases: Hope for the Future. *Cell* **181**, 168–188 (2020).

957 4. Kruk, S. K. *et al.* Vulnerability of pediatric patients with mitochondrial disease to vaccine-preventable
958 diseases. *J. Allergy Clin. Immunol. Pract.* **7**, 2415-2418.e3 (2019).
959 5. Walker, M. A. *et al.* Predisposition to infection and SIRS in mitochondrial disorders: 8 years'
960 experience in an academic center. *J. Allergy Clin. Immunol. Pract.* **2**, 465–468, 468.e1 (2014).
961 6. Eom, S. *et al.* Cause of Death in Children With Mitochondrial Diseases. *Pediatr. Neurol.* **66**, 82–88
962 (2017).
963 7. Jestin, M. *et al.* Mitochondrial disease disrupts hepatic allostasis and lowers the threshold for
964 immune-mediated liver toxicity. *Mol. Metab.* **37**, 100981 (2020).
965 8. West, A. P., Shadel, G. S. & Ghosh, S. Mitochondria in innate immune responses. *Nat. Rev. Immunol.*
966 **11**, 389–402 (2011).
967 9. West, A. P. Mitochondrial dysfunction as a trigger of innate immune responses and inflammation.
968 *Toxicology* **391**, 54–63 (2017).
969 10. West, A. P. & Shadel, G. S. Mitochondrial DNA in innate immune responses and inflammatory
970 pathology. *Nat. Rev. Immunol.* **17**, 363–375 (2017).
971 11. Warren, E. B. *et al.* Inflammatory and interferon gene expression signatures in patients with
972 mitochondrial disease. *J. Transl. Med.* **21**, 331 (2023).
973 12. Hasselmann, O. *et al.* Cerebral folate deficiency and CNS inflammatory markers in Alpers
974 disease. *Mol. Genet. Metab.* **99**, 58–61 (2010).
975 13. Wilson, L. D., Al-Majid, S., Rakovski, C. S. & Md, C. D. Higher IL-6 and IL6:IGF Ratio in Patients
976 with Barth Syndrome. *J. Inflamm.* **9**, 25 (2012).
977 14. Khan, W. *et al.* Neuroinflammation in the Cerebellum and Brainstem in Friedreich Ataxia: An [^{18}
978 F]- FEMPA PET Study. *Mov. Disord.* **37**, 218–224 (2022).
979 15. Nachun, D. *et al.* Peripheral blood gene expression reveals an inflammatory transcriptomic
980 signature in Friedreich's ataxia patients. *Hum. Mol. Genet.* **27**, 2965–2977 (2018).

981 16. Jin, Z., Wei, W., Yang, M., Du, Y. & Wan, Y. Mitochondrial Complex I Activity Suppresses
982 Inflammation and Enhances Bone Resorption by Shifting Macrophage-Osteoclast Polarization. *Cell*
983 *Metab.* **20**, 483–498 (2014).
984 17. Yu, A. K. *et al.* Mitochondrial complex I deficiency leads to inflammation and retinal ganglion cell
985 death in the Ndufs4 mouse. *Hum. Mol. Genet.* **24**, 2848–2860 (2015).
986 18. Stokes, J. C. *et al.* Leukocytes mediate disease pathogenesis in the Ndufs4(KO) mouse model of
987 Leigh syndrome. *JCI Insight* **7**, e156522 (2022).
988 19. Hanaford, A. & Johnson, S. C. The immune system as a driver of mitochondrial disease
989 pathogenesis: a review of evidence. *Orphanet J. Rare Dis.* **17**, 335 (2022).
990 20. Lei, Y. *et al.* Elevated type I interferon responses potentiate metabolic dysfunction,
991 inflammation, and accelerated aging in mtDNA mutator mice. *Sci. Adv.* **7**, eabe7548 (2021).
992 21. Saha, S., Buttari, B., Panieri, E., Profumo, E. & Saso, L. An Overview of Nrf2 Signaling Pathway
993 and Its Role in Inflammation. *Mol. Basel Switz.* **25**, 5474 (2020).
994 22. Nezu, M., Suzuki, N. & Yamamoto, M. Targeting the KEAP1-NRF2 System to Prevent Kidney
995 Disease Progression. *Am. J. Nephrol.* **45**, 473–483 (2017).
996 23. Trifunovic, A. *et al.* Premature ageing in mice expressing defective mitochondrial DNA
997 polymerase. *Nature* **429**, 417–423 (2004).
998 24. Kujoth, G. C. *et al.* Mitochondrial DNA mutations, oxidative stress, and apoptosis in mammalian
999 aging. *Science* **309**, 481–484 (2005).
1000 25. Chen, M. L. *et al.* Erythroid dysplasia, megaloblastic anemia, and impaired lymphopoiesis arising
1001 from mitochondrial dysfunction. *Blood* **114**, 4045–4053 (2009).
1002 26. Thomsen, K. *et al.* Animal models of chronic and recurrent Pseudomonas aeruginosa lung
1003 infection: significance of macrolide treatment. *APMIS Acta Pathol. Microbiol. Immunol. Scand.* **130**,
1004 458–476 (2022).

1005 27. Lavoie, E. G., Wangdi, T. & Kazmierczak, B. I. Innate immune responses to Pseudomonas
1006 aeruginosa infection. *Microbes Infect.* **13**, 1133–1145 (2011).
1007 28. Lister, P. D., Wolter, D. J. & Hanson, N. D. Antibacterial-resistant Pseudomonas aeruginosa:
1008 clinical impact and complex regulation of chromosomally encoded resistance mechanisms. *Clin.*
1009 *Microbiol. Rev.* **22**, 582–610 (2009).
1010 29. Lambert, M.-L. *et al.* Clinical outcomes of health-care-associated infections and antimicrobial
1011 resistance in patients admitted to European intensive-care units: a cohort study. *Lancet Infect. Dis.*
1012 **11**, 30–38 (2011).
1013 30. Hayashi, G. *et al.* Dimethyl fumarate mediates Nrf2-dependent mitochondrial biogenesis in mice
1014 and humans. *Hum. Mol. Genet.* **26**, 2864–2873 (2017).
1015 31. Robledinos-Antón, N., Fernández-Ginés, R., Manda, G. & Cuadrado, A. Activators and Inhibitors
1016 of NRF2: A Review of Their Potential for Clinical Development. *Oxid. Med. Cell. Longev.* **2019**,
1017 9372182 (2019).
1018 32. Hoyle, C., Green, J. P., Allan, S. M., Brough, D. & Lemarchand, E. Itaconate and fumarate
1019 derivatives inhibit priming and activation of the canonical NLRP3 inflammasome in macrophages.
1020 *Immunology* **165**, 460–480 (2022).
1021 33. Sutterwala, F. S. *et al.* Immune recognition of Pseudomonas aeruginosa mediated by the
1022 IPAF/NLRC4 inflammasome. *J. Exp. Med.* **204**, 3235–3245 (2007).
1023 34. Balakrishnan, A., Karki, R., Berwin, B., Yamamoto, M. & Kanneganti, T.-D. Guanylate binding
1024 proteins facilitate caspase-11-dependent pyroptosis in response to type 3 secretion system-negative
1025 Pseudomonas aeruginosa. *Cell Death Discov.* **4**, 66 (2018).
1026 35. Arlehamn, C. S. L. & Evans, T. J. Pseudomonas aeruginosa pilin activates the inflammasome. *Cell.*
1027 *Microbiol.* **13**, 388–401 (2011).

1028 36. Billingham, L. K. *et al.* Mitochondrial electron transport chain is necessary for NLRP3
1029 inflammasome activation. *Nat. Immunol.* **23**, 692–704 (2022).
1030 37. Kumari, P., Russo, A. J., Wright, S. S., Muthupalani, S. & Rathinam, V. A. Hierarchical cell-type-
1031 specific functions of caspase-11 in LPS shock and antibacterial host defense. *Cell Rep.* **35**, 109012
1032 (2021).
1033 38. Benjamin, J. T. *et al.* IL-1α and Not IL-1β Drives IL-1R1–Dependent Neonatal Murine Sepsis
1034 Lethality. *J. Immunol.* **201**, 2873–2878 (2018).
1035 39. Pyrillou, K., Burzynski, L. C. & Clarke, M. C. H. Alternative Pathways of IL-1 Activation, and Its
1036 Role in Health and Disease. *Front. Immunol.* **11**, 613170 (2020).
1037 40. Rathinam, V. A. K. *et al.* TRIF Licenses Caspase-11-Dependent NLRP3 Inflammasome Activation
1038 by Gram-Negative Bacteria. *Cell* **150**, 606–619 (2012).
1039 41. Kim, B.-H. *et al.* A family of IFN-γ-inducible 65-kD GTPases protects against bacterial infection.
1040 *Science* **332**, 717–721 (2011).
1041 42. Kim, B.-H. *et al.* Interferon-induced guanylate-binding proteins in inflammasome activation and
1042 host defense. *Nat. Immunol.* **17**, 481–489 (2016).
1043 43. Shenoy, A. R. *et al.* GBP5 promotes NLRP3 inflammasome assembly and immunity in mammals.
1044 *Science* **336**, 481–485 (2012).
1045 44. Coers, J. Sweet host revenge: Galectins and GBPs join forces at broken membranes. *Cell.*
1046 *Microbiol.* **19**, e12793 (2017).
1047 45. Lam, C.-W. *et al.* Novel POLG mutation in a patient with sensory ataxia, neuropathy,
1048 ophthalmoparesis and stroke. *Clin. Chim. Acta Int. J. Clin. Chem.* **448**, 211–214 (2015).
1049 46. Amiot, A. *et al.* Frequency of mitochondrial defects in patients with chronic intestinal pseudo-
1050 obstruction. *Gastroenterology* **137**, 101–109 (2009).

1051 47. Kinoshita, M. & Sawa, T. Serological immune response against major secretory proteins
1052 expressed by Pseudomonas aeruginosa upon intratracheal infection in mice. *Respir. Investig.* **60**, 318–
1053 321 (2022).
1054 48. Edmonds, J. L. *et al.* The Otolaryngological Manifestations of Mitochondrial Disease and the Risk
1055 of Neurodegeneration With Infection. *Arch. Otolaryngol. Neck Surg.* **128**, 355 (2002).
1056 49. Lee, W. S. & Sokol, R. J. Mitochondrial Hepatopathies: Advances in Genetics, Therapeutic
1057 Approaches, and Outcomes. *J. Pediatr.* **163**, 942–948 (2013).
1058 50. The Mitochondrial Medicine Society *et al.* A modern approach to the treatment of mitochondrial
1059 disease. *Curr. Treat. Options Neurol.* **11**, 414–430 (2009).
1060 51. Rahman, S. & Copeland, W. C. POLG-related disorders and their neurological manifestations.
1061 *Nat. Rev. Neurol.* **15**, 40–52 (2019).
1062 52. Gaudó, P. *et al.* Infectious stress triggers a POLG-related mitochondrial disease. *neurogenetics*
1063 **21**, 19–27 (2020).
1064 53. Al-Zubeidi, D. *et al.* Fatal Human Herpesvirus 6–Associated Encephalitis in Two Boys With
1065 Underlying POLG Mitochondrial Disorders. *Pediatr. Neurol.* **51**, 448–452 (2014).
1066 54. Torres-Odio, S. *et al.* Loss of Mitochondrial Protease CLPP Activates Type I IFN Responses
1067 through the Mitochondrial DNA-cGAS-STING Signaling Axis. *J. Immunol. Baltim. Md 1950* **206**, 1890–
1068 1900 (2021).
1069 55. Kobayashi, E. H. *et al.* Nrf2 suppresses macrophage inflammatory response by blocking
1070 proinflammatory cytokine transcription. *Nat. Commun.* **7**, 11624 (2016).
1071 56. Seidel, P. *et al.* Dimethylfumarate inhibits NF-κB function at multiple levels to limit airway
1072 smooth muscle cell cytokine secretion. *Am. J. Physiol.-Lung Cell. Mol. Physiol.* **297**, L326–L339 (2009).
1073 57. Hu, H. *et al.* Dimethyl fumarate covalently modifies Cys673 of NLRP3 to exert anti-inflammatory
1074 effects. *iScience* **27**, 109544 (2024).

1075 58. Humphries, F. *et al.* Succination inactivates gasdermin D and blocks pyroptosis. *Science* **369**,
1076 1633–1637 (2020).
1077 59. Miao, R. *et al.* Gasdermin D permeabilization of mitochondrial inner and outer membranes
1078 accelerates and enhances pyroptosis. *Immunity* **56**, 2523-2541.e8 (2023).
1079 60. Miao, N. *et al.* Oxidized mitochondrial DNA induces gasdermin D oligomerization in systemic
1080 lupus erythematosus. *Nat. Commun.* **14**, 872 (2023).
1081 61. Weindel, C. G. *et al.* Mitochondrial ROS promotes susceptibility to infection via gasdermin D-
1082 mediated necroptosis. *Cell* **185**, 3214-3231.e23 (2022).
1083 62. Moretti, J. *et al.* Caspase-11 interaction with NLRP3 potentiates the noncanonical activation of
1084 the NLRP3 inflammasome. *Nat. Immunol.* **23**, 705–717 (2022).
1085 63. Yazdi, A. S. & Drexler, S. K. Regulation of interleukin 1α secretion by inflammasomes: Table 1.
1086 *Ann. Rheum. Dis.* **72**, ii96–ii99 (2013).
1087 64. Kang, Y. *et al.* Ancestral allele of DNA polymerase gamma modifies antiviral tolerance. *Nature*
1088 **628**, 844–853 (2024).
1089 65. Liu, B. C. *et al.* Constitutive Interferon Maintains GBP Expression Required for Release of
1090 Bacterial Components Upstream of Pyroptosis and Anti-DNA Responses. *Cell Rep.* **24**, 155-168.e5
1091 (2018).
1092 66. Dickinson, M. S. *et al.* LPS-aggregating proteins GBP1 and GBP2 are each sufficient to enhance
1093 caspase-4 activation both in cellulo and in vitro. *Proc. Natl. Acad. Sci.* **120**, e2216028120 (2023).
1094 67. Pilla, D. M. *et al.* Guanylate binding proteins promote caspase-11–dependent pyroptosis in
1095 response to cytoplasmic LPS. *Proc. Natl. Acad. Sci.* **111**, 6046–6051 (2014).
1096 68. Meunier, E. *et al.* Caspase-11 activation requires lysis of pathogen-containing vacuoles by IFN-
1097 induced GTPases. *Nature* **509**, 366–370 (2014).

1098 69. Bezbradica, J. S., Coll, R. C. & Boucher, D. Activation of the Non-canonical Inflammasome in
1099 Mouse and Human Cells. in *The Inflammasome* (ed. Abdul-Sater, A. A.) vol. 2459 51–63 (Springer US,
1100 New York, NY, 2022).
1101 70. Kamajaya, L. J. & Boucher, D. Gasdermin D Cleavage Assay Following Inflammasome Activation.
1102 in *The Inflammasome* (ed. Abdul-Sater, A. A.) vol. 2459 39–49 (Springer US, New York, NY, 2022).
1103
1104

Fig. 1

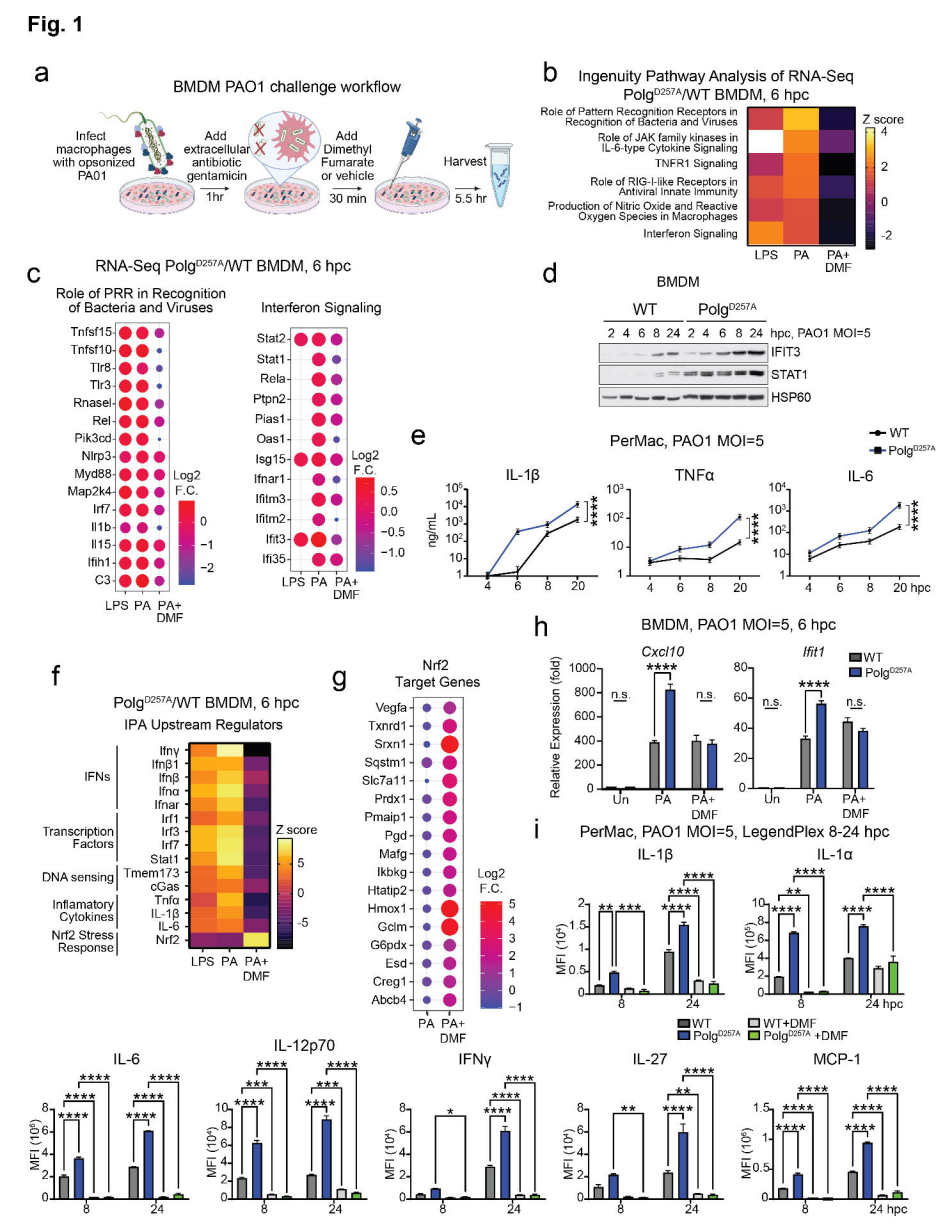
a
BMDM PAO1 challenge workflow
Infect macrophages with opsonized PA01
Add extracellular antibiotic gentamicin
1hr
Add Dimethyl Fumarate or vehicle
30 min
Harvest
5.5 hr
b
Ingenuity Pathway Analysis of RNA-Seq
PolgD257A/WT BMDM, 6 hpc
Role of Pattern Recognition Receptors in Recognition of Bacteria and Viruses
Role of JAK family kinases in IL-6-type Cytokine Signaling
TNFR1 Signaling
Role of RIG-I-like Receptors in Antiviral Innate Immunity
Production of Nitric Oxide and Reactive Oxygen Species in Macrophages
Interferon Signaling
LPS
PA
PA+ DMF
Z score
c
RNA-Seq PolgD257A/WT BMDM, 6 hpc
Role of PRR in Recognition of Bacteria and Viruses
Tnfsf15
Tnfsf10
Tlr8
Tlr3
Rnasel
Rel
Pik3cd
Nlrp3
Myd88
Map2k4
Irf7
Il1b
Il15
Ifih1
C3
Interferon Signaling
Stat2
Stat1
Rela
Ptpn2
Pias1
Oas1
Isg15
Ifnar1
Ifitm3
Ifitm2
Ifit3
Ifi35
Log2 F.C.
LPS PA PA+ DMF
d
BMDM
WT
PolgD257A
2 4 6 8 24 2 4 6 8 24 hpc, PAO1 MOI=5
IFIT3
STAT1
HSP60
e
PerMac, PAO1 MOI=5
WT
PolgD257A
IL-1β
TNFα
IL-6
ng/mL
20 hpc
h
BMDM, PAO1 MOI=5, 6 hpc
Cxcl10
Ifit1
Relative Expression (fold)
n.s.
Un PA PA+ DMF
f
PolgD257A/WT BMDM, 6 hpc
IPA Upstream Regulators
IFNs
Ifnγ
Ifnβ1
Ifnβ
Ifnα
Ifnar
Transcription Factors
Irf1
Irf3
Irf7
Stat1
DNA sensing
Tmem173
cGas
Inflamatory Cytokines
Tnfα
IL-1β
IL-6
Nrf2 Stress Response
Nrf2
Z score
g
Nrf2 Target Genes
Vegfa
Txnrd1
Srxn1
Sqstm1
Slc7a11
Prdx1
Pmaip1
Pgd
Mafg
Ikbkg
Hmox1
Gclm
G6pdx
Esd
Creg1
Abcb4
Log2 F.C.
PA PA+ DMF
i
PerMac, PAO1 MOI=5, LegendPlex 8-24 hpc
IL-1β
IL-1α
IL-6
IL-12p70
IFNγ
IL-27
MCP-1
MFI (10⁴)
8 24 24 hpc
WT
PolgD257A
WT+DMF
PolgD257A +DMF

Fig. 2

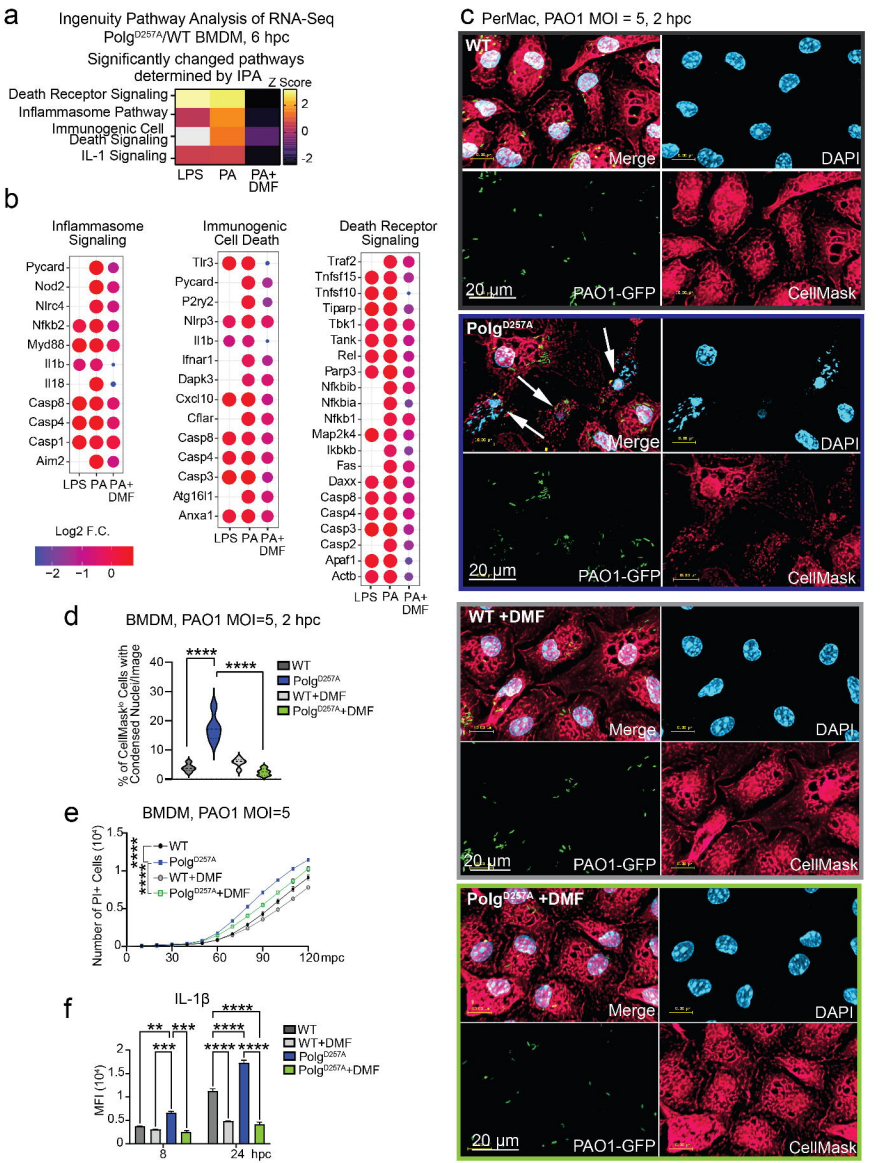
a
Ingenuity Pathway Analysis of RNA-Seq
PolgD257A/WT BMDM, 6 hpc
Significantly changed pathways determined by IPA
Z Score
Death Receptor Signaling
Inflammasome Pathway
Immunogenic Cell Death Signaling
IL-1 Signaling
LPS
PA
PA+ DMF
b
Inflammasome Signaling
Pycard
Nod2
Nlrc4
Nfkb2
Myd88
Il1b
Il18
Casp8
Casp4
Casp1
Aim2
Immunogenic Cell Death
Tlr3
Pycard
P2ry2
Nlrp3
Il1b
Ifnar1
Dapk3
Cxcl10
Cflar
Casp8
Casp4
Casp3
Atg16l1
Anxa1
Death Receptor Signaling
Traf2
Tnfsf15
Tnfsf10
Tiparp
Tbk1
Tank
Rel
Parp3
Nfkbib
Nfkbia
Nfkb1
Map2k4
Ikbkb
Fas
Daxx
Casp8
Casp4
Casp3
Casp2
Apaf1
Actb
LPS PA PA+ DMF
Log2 F.C.
−2 −1 0
d
BMDM, PAO1 MOI=5, 2 hpc
% of CellMaskhi Cells with Condensed Nucleiimage
****
****
WT
PolgD257A
WT+DMF
PolgD257A+DMF
e
BMDM, PAO1 MOI=5
Number of PI+ Cells (10⁴)
WT
PolgD257A
WT+DMF
PolgD257A+DMF
0 30 60 90 120mpc
f
IL-1β
MFI (10⁴)
**
***
****
WT
WT+DMF
PolgD257A
PolgD257A+DMF
8
24 hpc
C PerMac, PAO1 MOI = 5, 2 hpc
WT
Merge
DAPI
20 µm
PAO1-GFP
CellMask
PolgD257A
WT +DMF
PolgD257A +DMF

Fig. 3

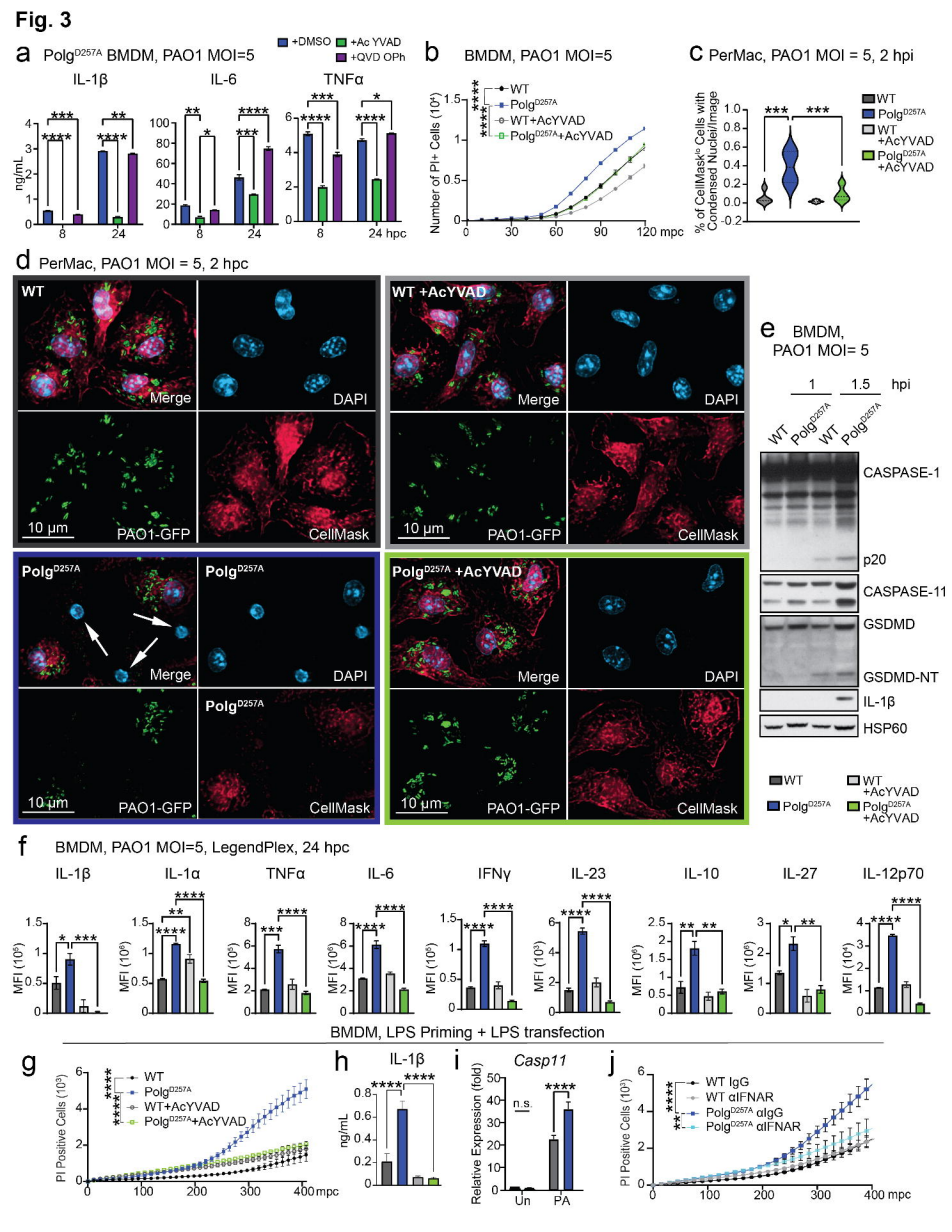

a Polg^{D257A} BMDM, PAO1 MOI=5
+DMSO
+Ac YVAD
+QVD OPh
IL-1β
IL-6
TNFα
ng/mL
24 hpc
b BMDM, PAO1 MOI=5
WT
Polg^{D257A}
WT+AcYVAD
Polg^{D257A}+AcYVAD
Number of PI+ Cells (10^4)
120 mpc
c PerMac, PAO1 MOI = 5, 2 hpi
% of CellMask^{lo} Cells with Condensed Nuclei/Image
d PerMac, PAO1 MOI = 5, 2 hpc
WT
WT +AcYVAD
Polg^{D257A}
Polg^{D257A} +AcYVAD
Merge
DAPI
PAO1-GFP
CellMask
10 μm
e BMDM, PAO1 MOI= 5
1
1.5
hpi
CASPASE-1
p20
CASPASE-11
GSDMD
GSDMD-NT
IL-1β
HSP60
f BMDM, PAO1 MOI=5, LegendPlex, 24 hpc
IL-1β
IL-1α
TNFα
IL-6
IFNγ
IL-23
IL-10
IL-27
IL-12p70
MFI (10^6)
MFI (10^4)
BMDM, LPS Priming + LPS transfection
g
PI Positive Cells (10^3)
400 mpc
h IL-1β
ng/mL
i Casp11
Relative Expression (fold)
n.s.
Un
PA
j
WT IgG
WT αIFNAR
Polg^{D257A} αIgG
Polg^{D257A} αIFNAR

Fig. 4

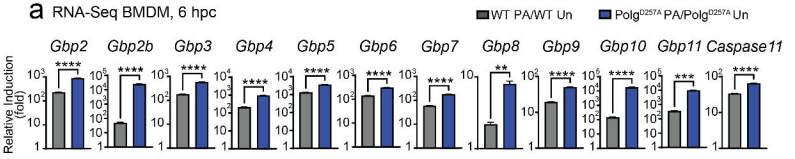
a RNA-Seq BMDM, 6 hpc
WT PA/WT Un
PolgD257A PA/PolgD257A Un
Gbp2
Gbp2b
Gbp3
Gbp4
Gbp5
Gbp6
Gbp7
Gbp8
Gbp9
Gbp10
Gbp11
Caspase11
Relative Induction (fold)
****
**
***

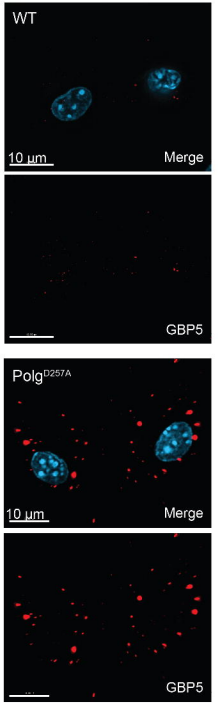
b BMDM, Unchallenged
WT
10 µm
Merge
GBP5
PolgD257A
10 µm
Merge
GBP5

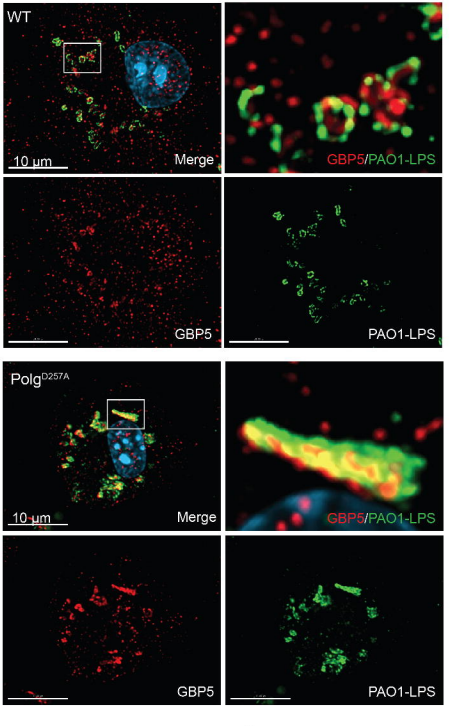
d BMDM, PAO1 MOI=5, 2 hpc
WT
10 µm
Merge
GBP5/PAO1-LPS
GBP5
PAO1-LPS
PolgD257A
10 µm
Merge
GBP5/PAO1-LPS
GBP5
PAO1-LPS

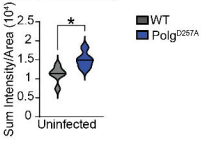
c
GBP5 intensity
Sum Intensity/Area (10⁴)
WT
PolgD257A
*
Uninfected

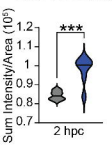
e
GBP5 intensity
Sum Intensity/Area (10⁵)
***
2 hpc

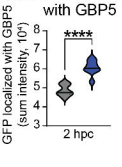
f
PAO1-LPS co-localized with GBP5
GFP localized with GBP5 (sum intensity, 10⁴)
****
2 hpc

Fig. 5

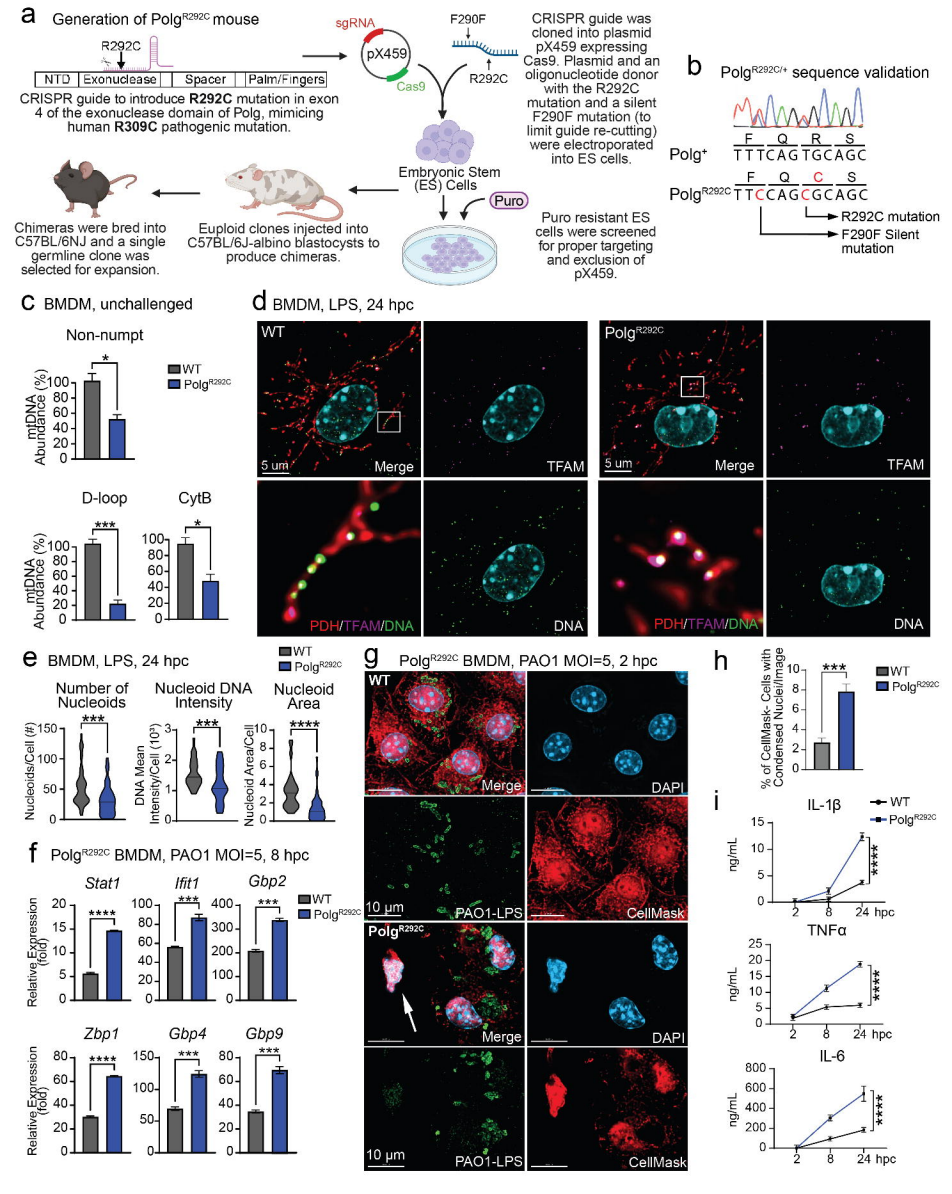
a
Generation of Polg^{R292C} mouse
R292C
NTD
Exonuclease
Spacer
Palm/Fingers
CRISPR guide to introduce R292C mutation in exon 4 of the exonuclease domain of Polg, mimicing human R309C pathogenic mutation.
sgRNA
pX459
Cas9
F290F
R292C
CRISPR guide was cloned into plasmid pX459 expressing Cas9. Plasmid and an oligonucleotide donor with the R292C mutation and a silent F290F mutation (to limit guide re-cutting) were electroporated into ES cells.
Embryonic Stem (ES) Cells
Puro
Puro resistant ES cells were screened for proper targeting and exclusion of pX459.
Euploid clones injected into C57BL/6J-albino blastocysts to produce chimeras.
Chimeras were bred into C57BL/6NJ and a single germline clone was selected for expansion.
b
Polg$^{R292C/+}$ sequence validation
F Q R S
Polg^{+} TTTCAGTGCAGC
F Q C S
Polg^{R292C} TTCCAGCGCAGC
R292C mutation
F290F Silent mutation
c
BMDM, unchallenged
Non-numpt
mtDNA Abundance (%)
WT
Polg^{R292C}
D-loop
CytB
d
BMDM, LPS, 24 hpc
WT
Polg^{R292C}
5 um
Merge
TFAM
PDH/TFAM/DNA
DNA
e
BMDM, LPS, 24 hpc
Number of Nucleoids
Nucleoids/Cell (#)
Nucleoid DNA Intensity
DNA Mean Intensity/Cell (10³)
Nucleoid Area
Nucleoid Area/Cell
f
Polg^{R292C} BMDM, PAO1 MOI=5, 8 hpc
Stat1
Ifit1
Gbp2
Zbp1
Gbp4
Gbp9
Relative Expression (fold)
g
Polg^{R292C} BMDM, PAO1 MOI=5, 2 hpc
WT
Polg^{R292C}
Merge
DAPI
10 µm
PAO1-LPS
CellMask
h
% of CellMask- Cells with Condensed Nucleii/image
i
IL-1β
TNFα
IL-6
ng/mL
2
8
24 hpc

Fig. 6

a BAL cytokines, LegendPlex, 1x10^4 CFU PAO1, 6 hpi

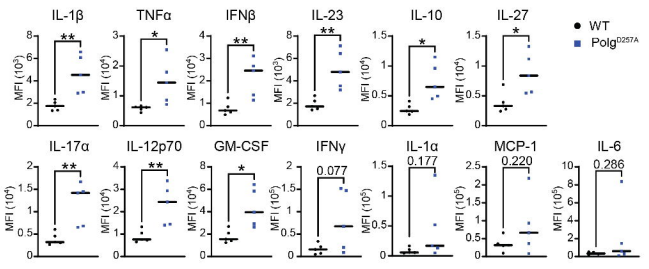

b Lung, 1x10^4 CFU PAO1, 48 hpi

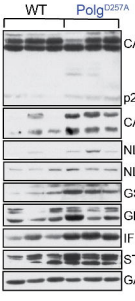

c Lung, 1x10^5 CFU PAO1, 20 hpi

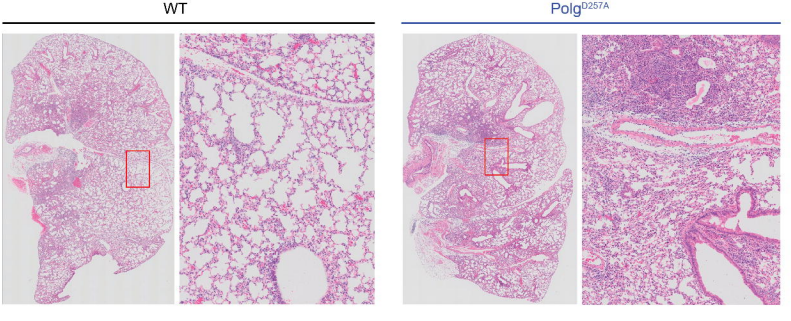

d Histology analysis, 1x10^5 CFU PAO1, 20 hpi

Genotype	ID	Total Inflammation	Neutrophilic Inflammation	Mononuclear Inflammation
WT	1	minimal	1	1
	2	minimal	0	1
	3	mild	2	1
	4	moderate	3	0
	5	mild	2	0
PolG	1	mild/moderate	2	0
	2	moderate	3	0
	3	moderate	3	0
	4	moderate	3	2
	5	severe	4	1

e 1x10^5 CFU PAO1, 20 hpi

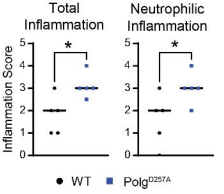

h

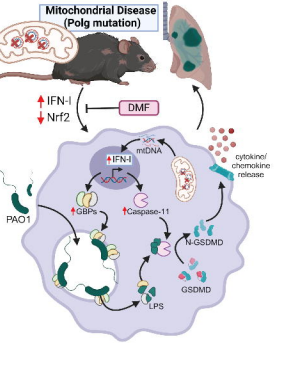

f 1x10^5 CFU PAO1, 20 hpi

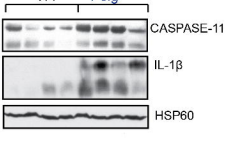

g 1x10^5 CFU PAO1

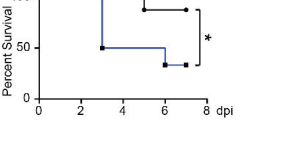

Supplementary Fig. 1

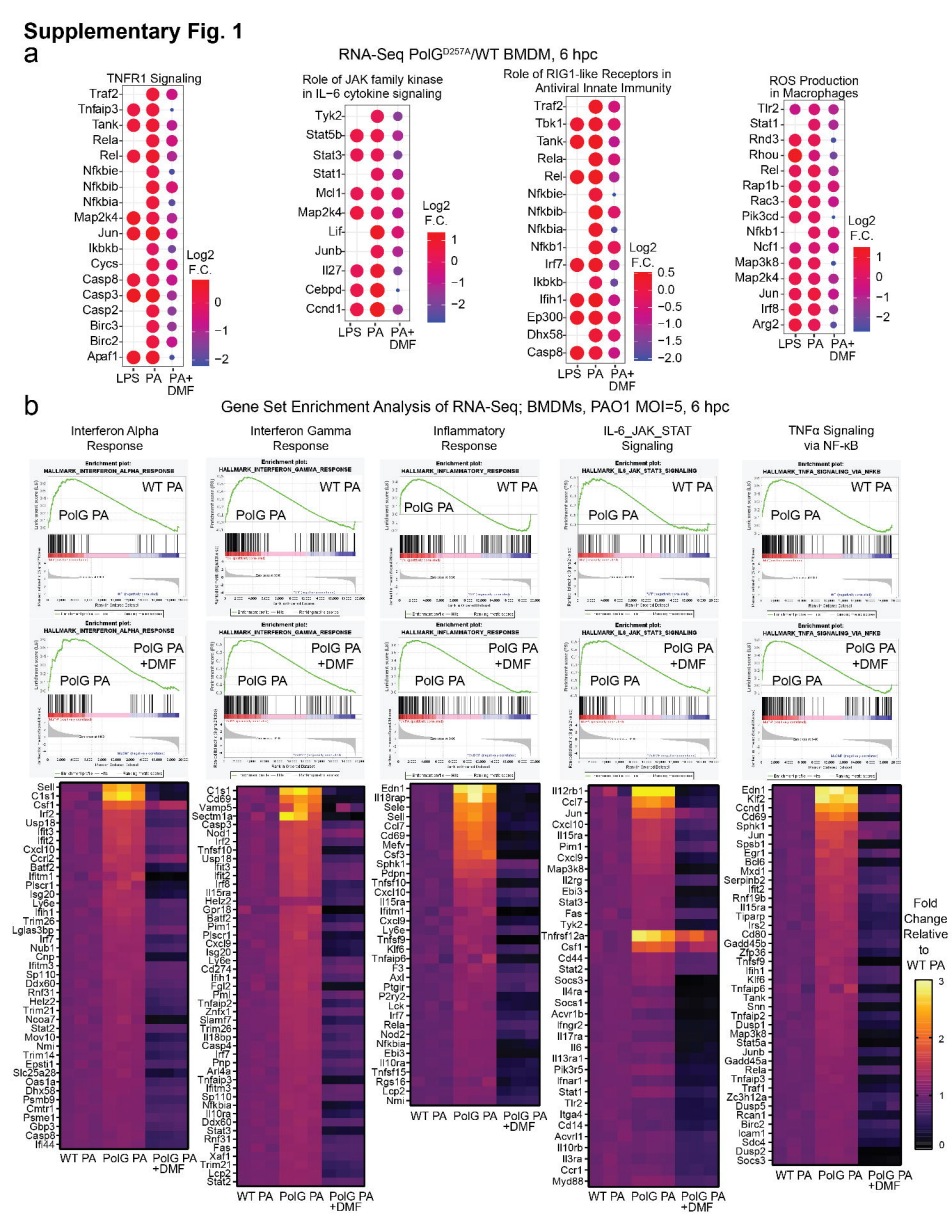

Supplementary Fig. 2

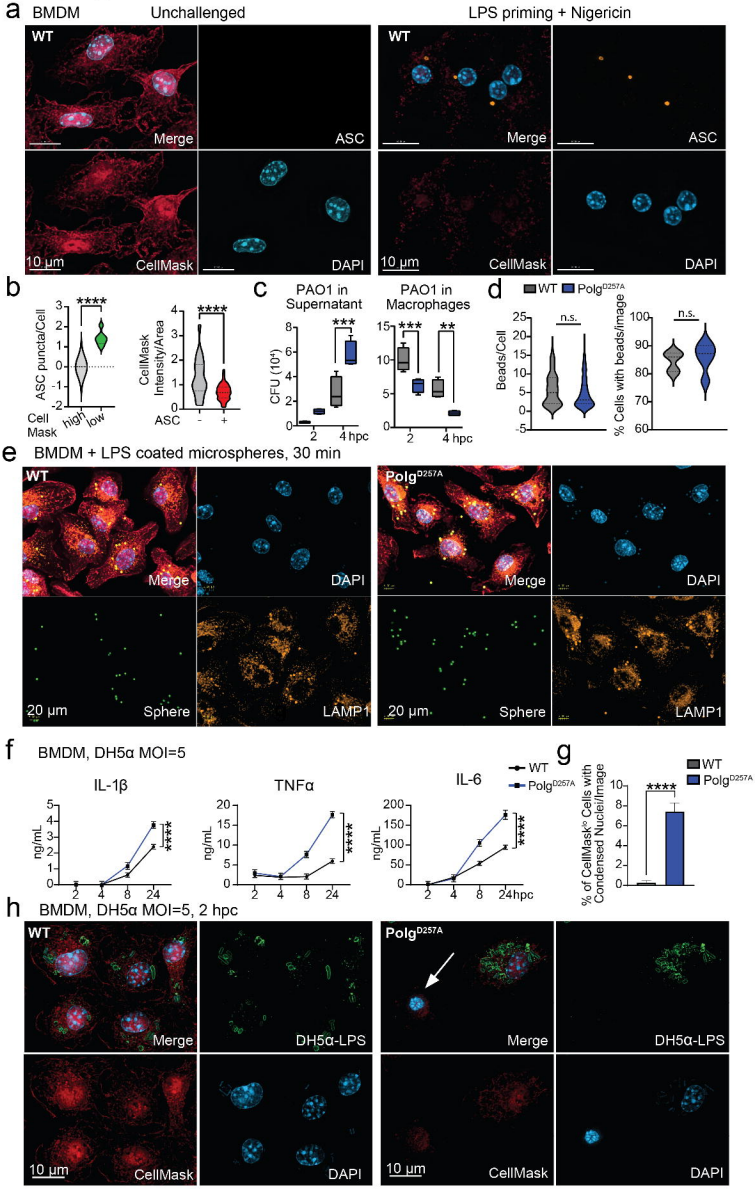

Supplementary Fig. 3

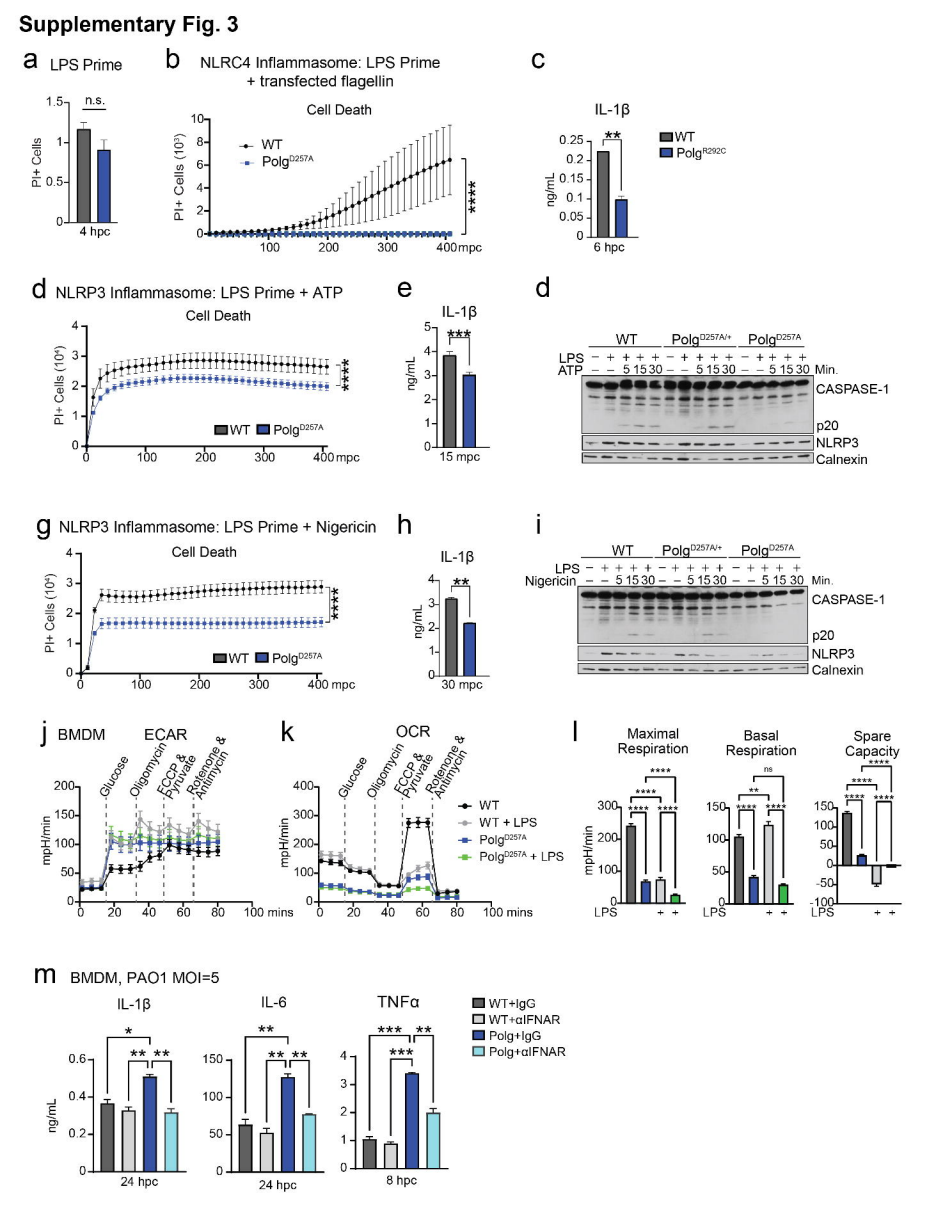

Supplementary Fig. 4

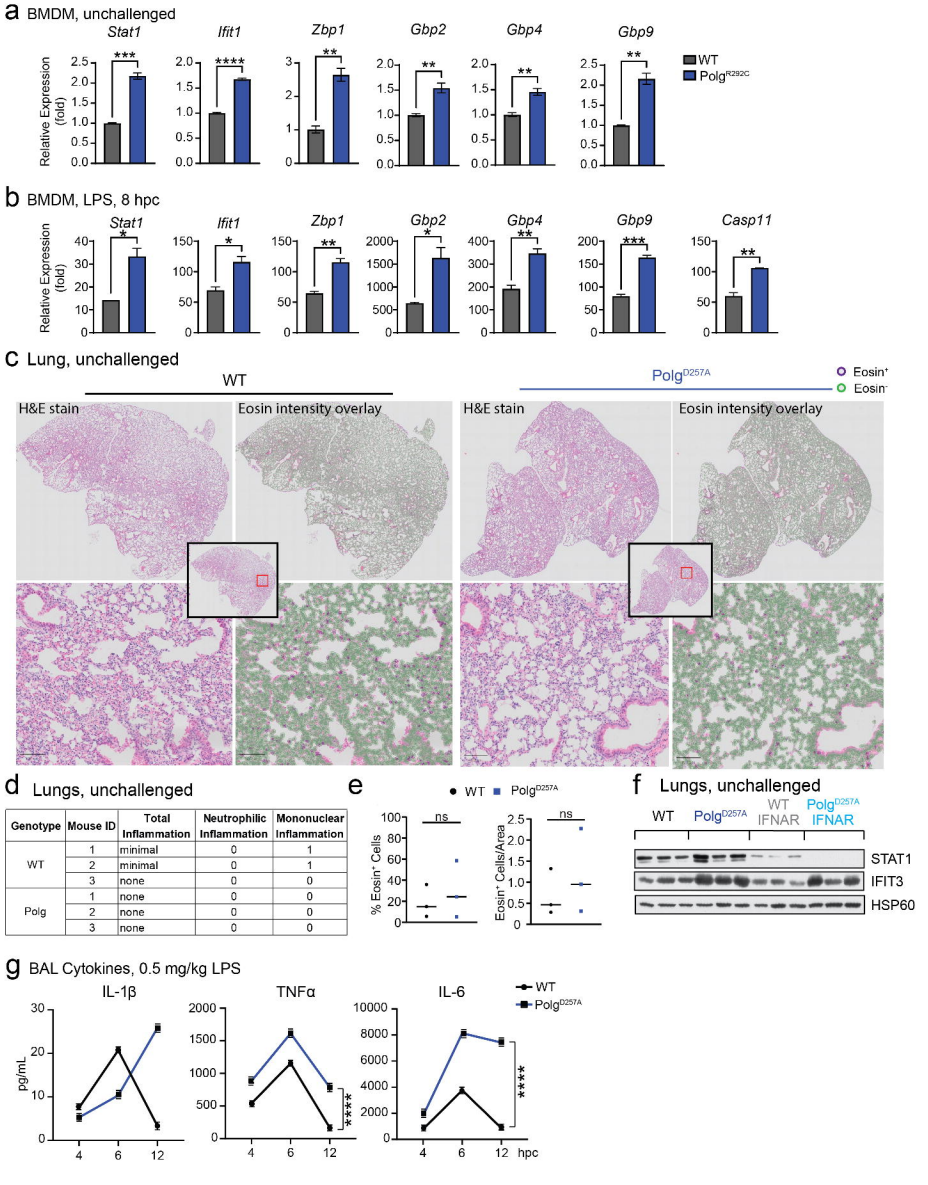

Genotype	Mouse ID	Total Inflammation	Neutrophilic Inflammation	Mononuclear Inflammation
WT	1	minimal	0	1
	2	minimal	0	1
	3	none	0	0
Polg	1	none	0	0
	2	none	0	0
	3	none	0	0

Supplementary Fig. 5

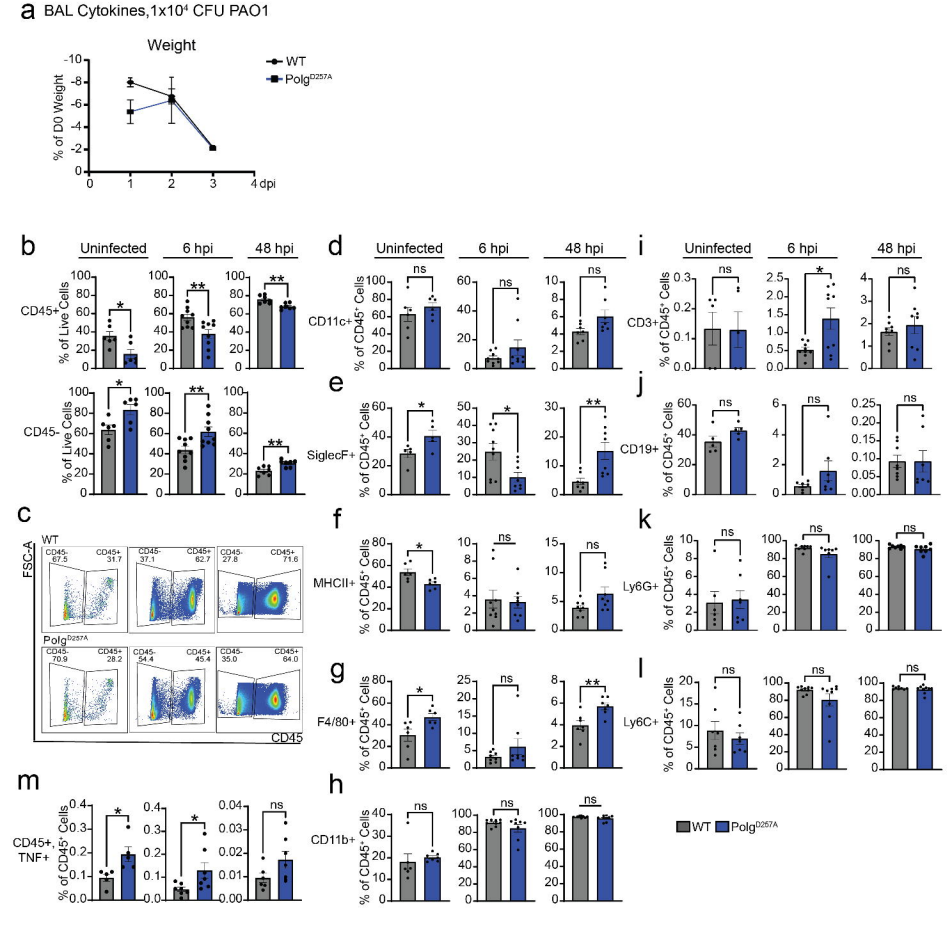
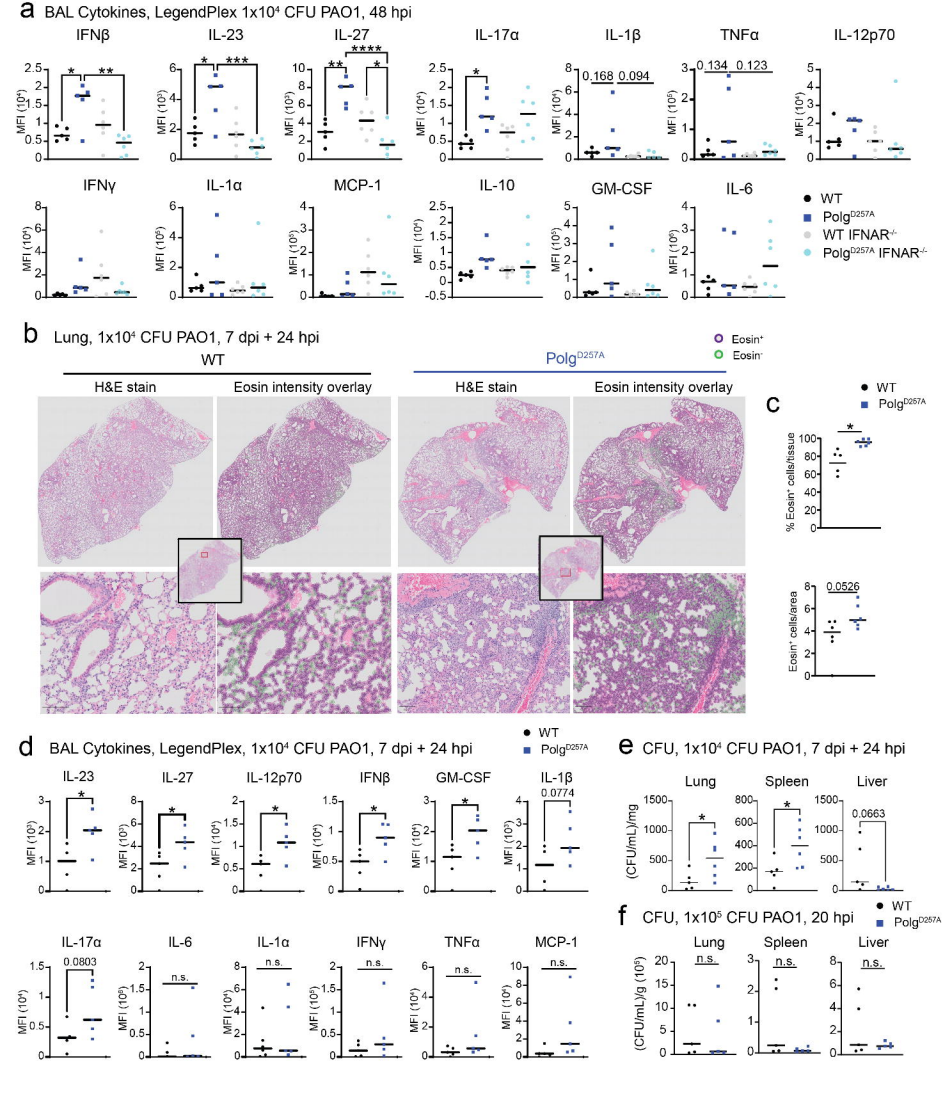
Supplementary Fig.6